Growth Kinetics and Microstructure of Gaseous Nitrided Iron Chromium Alloys

Ralf Erich Schacherl

Growth Kinetics and Microstructure of Gaseous Nitrided Iron Chromium Alloys

Von der Fakultät für Chemie der Universität Stuttgart

zur Erlangung der Würde eines Doktors der Naturwissenschaften (Dr. rer. nat.)

genehmigte Abhandlung

Vorgelegt von

Ralf Erich Schacherl

geb. in Künzelsau

Hauptberichter: Prof. Dr. Ir. E.J. Mittemeijer

Mitberichter: Prof. Dr. Ir. M.A.J. Somers

Mitprüfer: Prof. Dr. rer. nat. F. Aldinger

Tag der mündlichen Prüfung: 19.04.2004

MAX-PLANCK-INSTITUT FÜR METALLFORSCHUNG STUTTGART

INSTITUT FÜR METALLKUNDE DER UNIVERSITÄT STUTTGART

Stuttgart 2004

Table of Contents

1. Introduction

Nitriding as a method to improve the fatigue, corrosion and/or tribological properties of steel workpieces, is applied in very many cases in practise [1, 2]. Nitriding is a process where nitrogen is taken up in the surface-near regions of the workpieces.
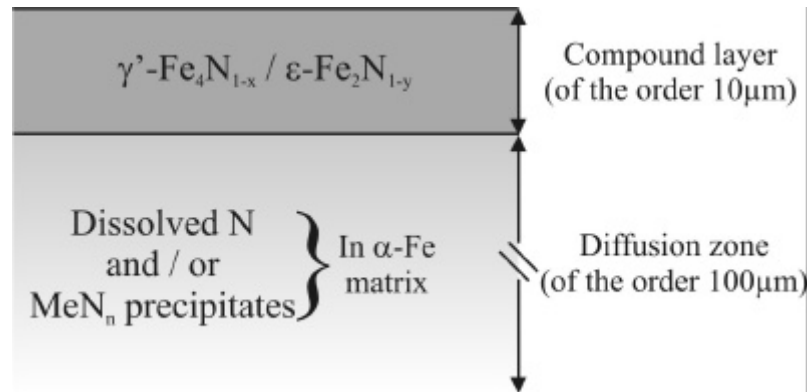
Fig. 1.1: Schematic presentation of the surface region of a nitrided piece of iron/iron-based alloy

Usually the nitrided surface region is subdivided into the compound layer adjacent to the surface, largely composed of iron nitrides, and the diffusion zone, where at the nitriding temperature the nitrogen is either dissolved (carbon steals) or precipitated as alloying element nitrides (alloyed steels) (see Fig. 2.9). The compound layer can be beneficial for the resistance against wear and corrosion. The diffusion zone brings about a strong increase of the fatigue resistance and also increases the wear resistance.

To introduce nitrogen in to iron-based alloys, several physical and chemical methods are available. The most commonly used methods are ion nitriding, salt bath nitrocarburising or the classical gaseous nitriding (see also ref. [2] page 71ff.). In this work gaseous nitriding was applied, because this method allows precise control of the chemical potential of nitrogen in the nitriding atmosphere.

Gaseous nitriding involves a gas-metal reaction where the metallic sample is suspended in a furnace usually containing a (flowing) NH_3/H_2 gas mixture. The chemical potential of a gas component in a gas mixture is defined as

$$\boldsymbol{m}_{i,g} = \boldsymbol{m}_{i,g}^{o} + RT\ln\left(\frac{f_i}{f_i^{o}}\right) \qquad (1)$$

where $\boldsymbol{m}_{i,g}^{o}$ is the chemical potential of i in the gaseous reference state, f_i the fugacity of the component i in the gas mixture, and f_i^o the fugacity of i in the reference state. If ideal gases are assumed, Eq. (1) becomes

$$\boldsymbol{m}_{i,g} = \boldsymbol{m}_{i,g}^{o} + RT\ln\left(\frac{p_i}{p_i^o}\right) \tag{2}$$

where p_i is the partial pressure of the component i in the gas mixture, and p_i^o the pressure of component i in the reference state. The chemical potential of an element or compound dissolved in the solid matrix is defined as

$$\boldsymbol{m}_{i,s} = \boldsymbol{m}_{i,s}^{o} + RT\ln a_i \tag{3}$$

where $\boldsymbol{m}_{i,s}^{o}$ denotes the chemical potential of the component i in the solid (s) reference state and, a_i represents the activity of i in the dissolved state with respect to the reference state (in the reference state $a_i=1$).

The reaction which takes place between the NH_3/H_2 gas atmosphere and an α-iron solid can be described as follows:

$$NH_3 \Leftrightarrow N_a + \frac{3}{2}H_2 \tag{4}$$

where N_α denotes the nitrogen dissolved in α-Fe. If equilibrium between metal and gas prevails, it follows on the basis of Eqs. (2)-(4) that the chemical potential of nitrogen dissolved in the solid, $\boldsymbol{m}_{N_a}$, obeys [3] :

$$\mu_N = \mu_{NH_3}^0 - \frac{3}{2}\mu_{H_2}^0 + RT\ln\left(\frac{p_{NH_3}}{p_{H_2}^{3/2}}\right) \tag{5}$$

Hence, the activity of nitrogen dissolved in the solid at a constant temperature is controlled by the ratio

$$r_n = \left(\frac{p_{NH_3}}{p_{H_2}^{3/2}}\right) \tag{6}$$

which is called nitriding potential (in German: Nitrierkennzahl). By controlling the composition of the gas mixture (mass flows of NH_3 and H_2) in the furnace, which is possible to a high degree of accuracy with well calibrated mass-flow controllers, the nitriding potential can be used as one of the decisive, independent variables of the nitriding process (next to temperature and time). By varying the gas mixture in the nitriding atmosphere and therefore

the activity of nitrogen in the solid three different iron-nitrogen phases can be produced upon nitriding iron, namely the hexagonal ε iron nitride, the cubic ordered γ' iron nitride and ferrite (α) with dissolved nitrogen on the octahedral interstitiel sites of the α-Fe bcc lattice. If the applied nitriding parameters (gas mixture and temperature) allows the formation of ε or γ' iron-nitrides, a compound layer is formed (see Fig.1.1) at the sample surface, where the phase with the highest amount of dissolved nitrogen is adjacent to the surface. Thus if the chosen nitriding parameters enable the formation of ε, the following sequence of iron – nitrogen phases will be obtained: ε, γ' in the compound layer at the surface with the diffusion zone underneath consisting of ferrite with dissolved nitrogen [3, 4].

Typical nitriding iron-based alloys contain elements as Mn, Cr, Al, Ti and V, which have a relatively strong chemical affinity to nitrogen. In these cases the formation and precipitation of nitrides can take place even if the chemical potential of nitrogen of the nitriding atmosphere is too low to form nitrides with iron during nitriding; i.e. r_n is below the critical value for compound-layer formation. This precipitation of MeN_n particles in the iron matrix is also called "inner nitriding". The present study is a contribution to the understanding of the nitriding behaviour of ferritic Fe-Cr alloys.

The formation of chromium nitride in α ferrite matrix occurs in different stages. In the initial stage fine precipitates with coherent or partly coherent interfaces with the iron matrix develop. In the diffusion zone this precipitation stage can be observed usually at relatively large depths, consequently to the "youngest" part of the diffusion zone (indicated as zone II in Fig. 1.2), i.e. near the interface between the nitrided zone (diffusion zone) and the not nitrided core. At this stage a relatively high hardness occurs due to long range strain fields induced by the misfit between the formed chromium-nitride particles and the iron matrix.
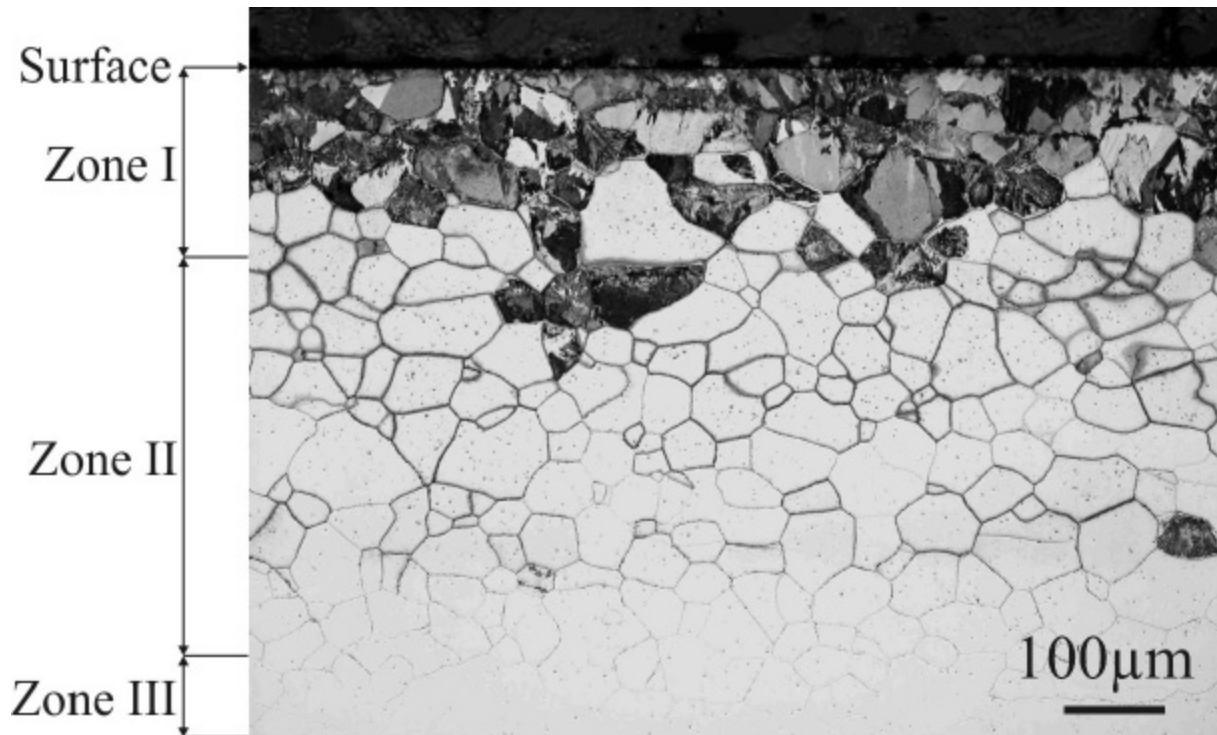
Fig. 1.2: Precipitation morphology of a nitrided zone of a Fe-7wt.%Cr alloy nitrided for 20h at r_n=0.1 (optical micrograph of the cross section of the nitrided layer). Zone I: region with grain exhibiting the discontinuous coarsening reaction; zone II: region of coherent, submicroscopical precipitation; zone III: unnitrided core.

On prolonged nitriding (in fact aging for the already nitrided region) a next stage of the precipitation process occurs: coarsening. Here two coarsening mechanisms can be indicated: (i) growth of individual precipitates, and (ii) an unusual discontinuous coarsening reaction leading to a lamellae-like morphology. This precipitation state can be observed usually in the "older" part of the diffusion zone, i.e. near to the sample surface. The discontinuously coarsened grains appear dark in the micrograph (see zone I in Fig. 1.2). Both coarsening mechanisms lead to loss of hardness.

An unusual and not fully understood phenomenon is the occurrence of excess nitrogen. Excess nitrogen is the amount of nitrogen which is taken up additionally to the amount of nitrogen due to the following contributions: (i) nitrogen which is bound in chromium nitride (in case of Fe-Cr alloys) and (ii) nitrogen which is dissolved in unstrained ferrite, according to the applied nitriding parameters (nitriding potential and nitriding temperature).

In the first part of this work (Chapter 2) the precipitation morphology of through nitrided samples (thin sheats) was investigated as function of the Cr content, the nitriding temperature and the nitriding potential. Contrary to common knowledge, it was shown that high Cr alloys can be nitrided. At relatively low temperature (<580°C) the discontinuous coarsening mechanism dominates. At higher nitriding temperatures a smaller number of grains experience the discontinuous coarsening. Samples nitrided at 700°C only exhibit the coarsening of the initially submicroscopical precipitates.

Excess nitrogen could be observed in all samples. On prolonged nitriding the capacity for excess nitrogen uptake vanishes and during the coarsening stage (part of the) excess nitrogen segregates and forms to N_2 pores near to large CrN particles.

In the second part of this work (chapter 3) the nitriding kinetics were investigated. In particular the focus of the attention was on the role of the excess nitrogen. For the first time it was possible to demonstrate that mobile and immobile excess nitrogen occur which have different effects on the growth kinetics of the nitrided zone. Eventually, as a result, a quantitative, numerical model could be vised that provides a realistic description of the growth kinetics of the nitrided zone.

Against the above sketched background the stimulus for this project can be summarized as follows:

  (i) To provide a fundamental understanding for the precipitation mechanism of MeN_n precipitates in ferritic iron.

 (ii) To explore the role of the excess nitrogen in the nitriding process and its effects on the resulting properties.

(iii) To develop a kinetic model that allows a quantitative description of the development of the nitrided zone.

Present-day, largely fragmented knowledge does not allow the constitution of a model, based on fundamental understanding, that could be used in nitriding practice to optimize the process and thus tune it for desired properties.

References

[1]   Mittemeijer, E.J.; Grosch, J. (eds.): AWT Berichtsband Nitrieren und Nitrocarburieren (1996).
[2]   Chatterjee-Fischer, R.: Wärmebehandlung von Eisenwerkstoffen, Expert Verlag, Renningen-Malmsheim (1995).
[3]   Mittemeijer, E.J.; Slycke, J.T.: Surface Eng. 12 (1996) 152.
[4]   Mittemeijer, E.J.; Somers, M.A.J.: Surface Eng. 13 (1997) 483.

2. Gaseous Nitriding of Iron-Chromium Alloys

R.E. Schacherl, P.C.J. Graat, E.J. Mittemeijer

Abstract

Fe-Cr alloys containing 4, 7, 13 and 20 wt.% chromium were nitrided in a gas mixture consisting of hydrogen and ammonia at temperatures of 450, 580 and 700 °C. To investigate the nitrided samples light microscopy, scanning electron microscopy, hardness measurements, X-ray diffraction, electron probe microanalysis (EPMA), and Auger electron spectroscopy were applied. The samples with 4 and 7 wt.% Cr which were nitrided at 450 and 580 °C exhibit grains of relatively high hardness, containing finely dispersed submicroscopical chromium nitride precipitates, as well as grains of lower hardness containing discontinuously precipitated chromium nitride. The samples nitrided at 700 °C contain relatively coarse CrN particles. All samples were completely nitrided (i.e., throughout the whole sample cross-section), as confirmed by EPMA: a constant nitrogen content, independent of the occurring precipitation morphology, was observed. This nitrogen content is larger than expected on the basis of the Cr content and the solubility of N in Fe: excess N occurs. Local Cr and N enrichment was observed near pores which had developed mainly along grain boundaries. These pores are especially present in the samples which were nitrided at 700 °C. The evolution of the precipitation morphology, the presence of excess N and the local enrichment of Cr and N near pores were discussed.

2.1 Introduction; current state of knowledge

Nitriding is a widespread method to improve the fatigue, tribological and/or corrosion properties of steel workpieces [1]. To obtain the desired properties of workpieces to be nitrided, it is necessary to acquire fundamental understanding of the processes which occur during nitriding. Parameters as the nitriding time, the nitriding temperature, and the nitriding potential are likely to play a key role [2-5]. Above all the microstructure of and the type of alloying elements in the steel are of cardinal importance [1, 3, 4, 6].

In the case of nitriding pure iron, layers of iron nitrides can be formed at the surface. Depending on the applied nitriding temperature and nitriding potential the hexagonal ε-Fe_2N_{1-z} and/or the cubic γ'-Fe_4N_{1-x} phases are formed [7]. If the nitriding conditions allow the formation of the ε phase (see Lehrer diagram [2, 5, 7]), it will be formed at the surface. The γ' phase can occur then as a second layer below the ε layer. Below the iron nitride layers always a zone of α-Fe with, at the nitriding temperature, nitrogen dissolved in the octahedral interstitial sites of the body-centred cubic Fe parent lattice is present: the so-called diffusion zone [7-14].

If Fe contains alloying elements with affinity for N, these elements will influence the formation of iron nitrides. Cr, for example, makes the formation of iron nitrides less likely because of the reduction of the N activity in the Fe matrix, whereas, for example, Si increases the tendency of formation of iron nitrides [3].

Cr is an alloying element that is often used in nitriding steels. Because of the relatively strong N–Cr interaction [3,15] chromium nitrides are formed (internal precipitation), which can increase the hardness of the material significantly. Chromium nitrides can occur in two modifications: face-centred cubic CrN and hexagonal Cr_2N. Which kind of chromium nitride is formed depends on the Cr content in the alloy [3,4]. Upon nitriding the formation of chromium nitride starts with the nucleation and growth of coherent or semicoherent chromium nitride precipitates [3, 4, 16, 17]. This stage is associated with relatively high hardness values because of the strain fields, induced by the misfit between chromium nitride and α-Fe [17]. On prolonged nitriding the chromium nitride precipitates coarsen and their number decreases, to reduce the Gibbs energy of the system by a decrease of the interfacial area between chromium nitride and α-Fe, and by a decrease (of the extent) of the stress fields surrounding the chromium nitride precipitates which become incoherent with the α-Fe matrix.

This ageing process reduces the hardness of the material. The coarsening of the chromium nitride precipitates could either take place by the continuous growth of the initial chromium nitride particles and/or by the (simultaneous) formation of chromium nitride and α-Fe lamellae (discontinuous precipitation). The discontinuous precipitation reaction initiates at grain boundaries. The discontinuously precipitated areas show relatively low hardness values because of the coarse microstructure and a (fully) relaxed misfit of the α-Fe/CrN interfaces [17,18].

Until now the focus of attention was on the gaseous nitriding of Fe-Cr alloys with relatively low Cr content (see, in particular, the articles cited above [6, 16, 17, 19]). Attention for the nitriding of Fe-based alloys with a relatively high Cr content has been scarce [4]. The gaseous nitriding of steels with high Cr content is known to be associated with problems caused by the presence of a chromium oxide layer at the surface of the alloy material before nitriding, which is thought to inhibit nitriding. In this work Fe-Cr alloys with up to 20 wt.% Cr have been nitrided in an NH_3/H_2 gas mixture at different temperatures. The nitrided specimens have been investigated with several techniques to analyse the microstructure, the phase constitution, the element distribution and the hardness.

2.2 Experimental

2.2.1 Specimen preparation

Fe-Cr alloys with nominally 4, 7, 13 and 20 wt.% Cr were prepared from pure Fe (99.98 wt.%) and pure Cr (99.999 wt.%) in an arc-melting furnace under argon atmosphere (99.999 vol.%). The amounts of oxygen, carbon and nitrogen impurities in the alloys were determined by chemical analysis (inductive-coupled plasma-optic emission spectroscopy), which yielded average values of 0.014 wt.% for oxygen, $6.3 \cdot 10^{-4}$ wt.% for carbon, and $<1 \cdot 10^{-4}$ wt.% for nitrogen. After melting, the alloys were cold rolled to sheets with a thickness between 150 and 200 µm (thickness reduction of 95 %). The obtained sheets were cut into rectangular pieces with an area of 2x2 cm^2 and subsequently encapsulated in a silica tube filled with argon (99.999 vol.%) up to 750 Torr. The encapsulated samples were annealed for 1 h at 700 °C to get a recrystallized grain structure. After annealing the grains had an average grain diameter of 36 µm. The hardness of the samples thus obtained was measured (load 50 g) yielding the following values: Fe-4Cr: 83 HV, Fe-7Cr: 97 HV, Fe-13Cr: 119 HV, Fe-20Cr: 156 HV. Electron probe microanalysis was used to verify that Cr was distributed

homogeneously in the sample. Before nitriding the samples were ground, polished (the last step being polishing with 1 µm diamond paste) and cleaned in an ultrasonic bath filled with ethanol.

2.2.2 Nitriding

For nitriding the specimen was suspended at a Pt wire in a vertical tube furnace (at the Technical University of Denmark). Initially, the specimens were annealed in a pure hydrogen atmosphere for 30 min at 750 °C. Subsequently the nitriding process was performed in the same furnace in a hydrogen/ammonia gas mixture. The fluxes of both gases were adjusted with mass flow controllers. The gas flows, nitriding temperatures and nitriding times applied have been given in Table 1. For the nitriding experiments that were performed at 450 and 580 °C the nitriding conditions were such that for pure Fe γ'-Fe4N would be obtained (see Lehrer diagram [5]). At the nitriding potential applied at 700 °C also the ε-Fe phase would be formed upon nitriding pure Fe. The nitriding time of about 18 h was chosen such that a complete nitriding of the samples should be obtained. However, the alloy with 4 wt.% Cr nitrided at 450 °C showed after 18 h a lower nitrogen content in the middle of the sample than near the surface and, therefore, another specimen of this alloy was nitrided for a longer time (55 h). After nitriding, the samples were cooled in a pure argon atmosphere down to room temperature in about 30 min.

Table 1: The nitriding parameters applied to the different alloys.

Alloy	Temperature (°C)	H$_2$ flow (ml/min)	NH$_3$ flow (ml/min)	Time (h)
Fe-4Cr	450	743	254	19 / 55
Fe-4Cr	580	875	122	16
Fe-4Cr	700	876	122	18
Fe-7Cr	450	743	254	19
Fe-7Cr	580	876	122	18
Fe-7Cr	700	876	122	18
Fe-13Cr	700	876	122	19
Fe-20Cr	700	876	122	19

2.2.3 Specimen Characterisation

2.2.3.1 Light microscopy

For light microscopical investigation, pieces were cut from the nitrided specimens with a diamond wire saw and prepared to cross-sections, by subsequent embedding (Konduktomet, Buehler GmbH), polishing (last step 1 μm diamond paste) and etching with 2.5 % nital (2.5 vol.% HNO_3 in ethanol) for about 5 s. Light micrographs were taken with a Leica DMRM microscope.

2.2.3.2 Scanning electron microscopy

For scanning electron microscopy (SEM) the same (etched) cross-sections were used as for light microscopy. The SEM micrographs were taken with a Jeol JSM 6300F operated at 3 or 5 kV.

2.2.3.3 Hardness measurement

Hardness measurements across the cross-sections of the nitrided specimens were performed with a Leitz Durimet hardness tester, applying a load of 50 g. The evaluated hardness values are average values of 5 to 10 measurements.

2.2.3.4 X-ray diffraction

To determine which phases are present after nitriding, XRD was applied using a Philips X'Pert diffractometer. Measurements were made employing Cu Kα radiation and the Bragg-Brentano geometry with a graphite monochromator in the diffracted beam. The diffraction angle range scanned was $2\Theta = 10 - 120°$ with a step size of 0.05°. The X-ray diffractograms were recorded from specimen surfaces as obtained after nitriding as well as from nitrided specimen from which surface material was removed by polishing, to get information about the phase depth distribution. To identify the phases from the diffraction peaks the data from the JCPDS data base were used [20].

2.2.3.5 Electron probe microanalysis (EPMA)

To determine the composition of the samples after nitriding, EPMA was performed employing a Cameca SX100 instrument. Cross-sections of the nitrided alloys similar to those as described above for light microscopy, were analysed, but in this case no etching after polishing was applied. A focussed electron beam at an accelerating voltage of 15 kV and a

current of 100 nA was applied. To obtain the element contents in the specimens, the intensity of the characteristic Fe Kβ, Cr Kβ, N Kα, and O Kα X-ray emission peaks was determined at points along lines across the cross-sections (single measurement points at a distance of 2 μm). The intensities obtained for the nitrided samples were divided by the intensities obtained from standard samples of pure Fe (Fe Kβ), pure Cr (Cr Kβ), andradite/$Ca_3Fe_2(SiO_4)_3$ (O Kα), and γ′-Fe_4N (N Kα). Concentration values were calculated from the intensity ratios applying the *F*(rz) approach according to Pouchou and Pichoir (PAP) [21].

2.2.3.6 Scanning Auger electron spectroscopy (AES)
To get more detailed information than possible with EPMA about the lateral variation (in the cross-section analyzed) of N contents near pores and grain boundaries AES analyses of the nitrided alloy with 13 wt.% Cr nitrided at 700 °C were performed employing a Phi 600 scanning Auger microscope. The instrument is equipped with a cylindrical mirror analyser and was operated at a relative energy resolution of 0.6 %. An electron beam with an accelerating voltage of 10 kV and beam currents of 6-30 nA was applied. Before analysis the area of interest was sputter cleaned applying 3 kV Ar^+ ions. Subsequently, the Fe LMM, Cr LMM, N KLL, O KLL, and C KLL Auger spectra were recorded at points along a line across a pore or grain boundary (single measurement points at a distance of 40 nm).

2.3 Results

2.3.1 Nitriding of Fe-4Cr and Fe-7Cr at 450 °C
Light micrographs of the cross-sections of the Fe-4Cr specimens nitrided at 450 °C are shown in Fig. 2.1. The Fe-4Cr specimens were nitrided for 19 and 55 h (Figs. 2.1a and b, respectively). Clearly, dark regions, mainly near the specimen surface, and bright regions, mainly in the centre of the specimen, can be observed. The sample, which was nitrided for the longer time has a higher content of dark areas, particularly in the centre region of the specimen. An enlargement of a region near a boundary between a dark and a bright region is shown in Fig. 2.2. The SEM micrograph (Fig. 2.2b) shows that the dark regions have a lamellae morphology, suggesting that discontinuous precipitation had occurred. The finest lamellae that can be observed have an inter lamellar spacing of 33 nm; the coarsest lamellae exhibit a spacing of 117 nm (not shown in Fig. 2.2). The nitrided Fe-7Cr alloy shows a

precipitation morphology in principle similar to the one observed for the Fe-4Cr alloy. However, for the nitrided Fe-7Cr alloys almost each grain contains discontinuously transformed regions (Fig.2.1c).
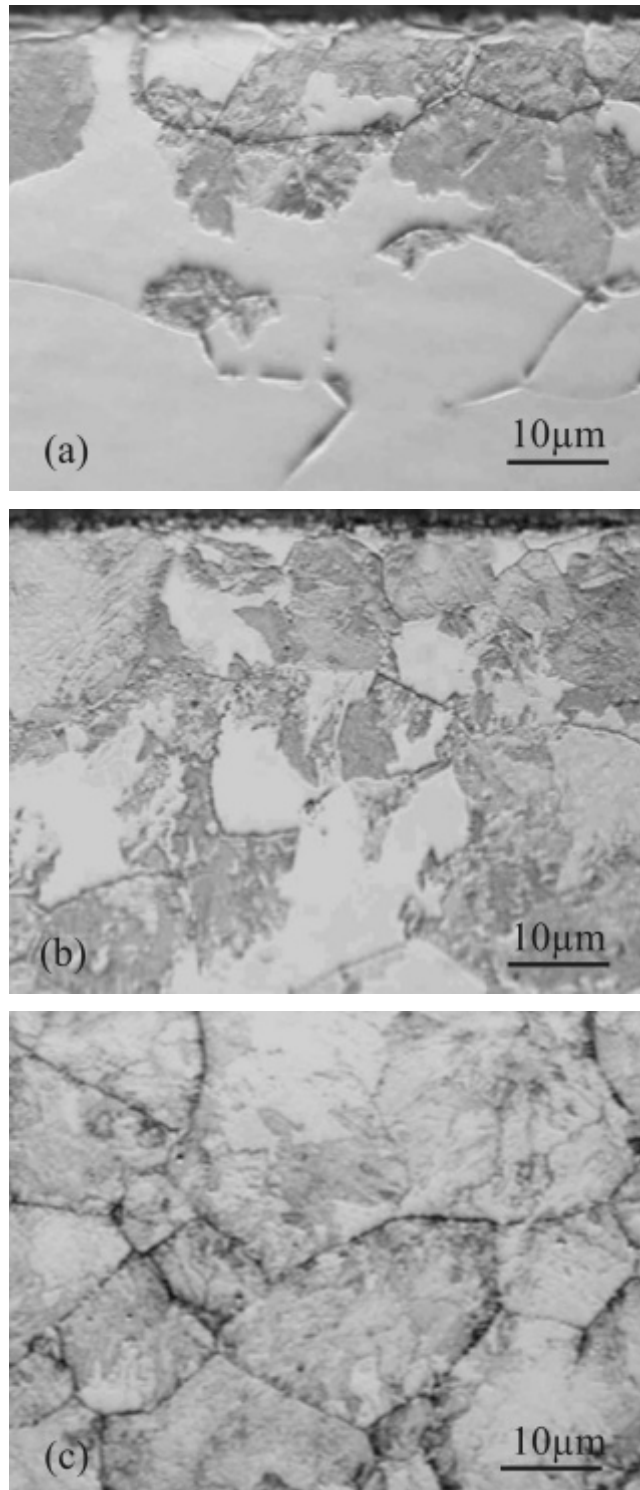

Fig. 2.1: Light micrograph of the Fe-4Cr alloy nitrided at 450 °C for 19 h (a), for 55 h (b), and of the Fe-7Cr alloy nitrided at 450 °C for 19 h (c).
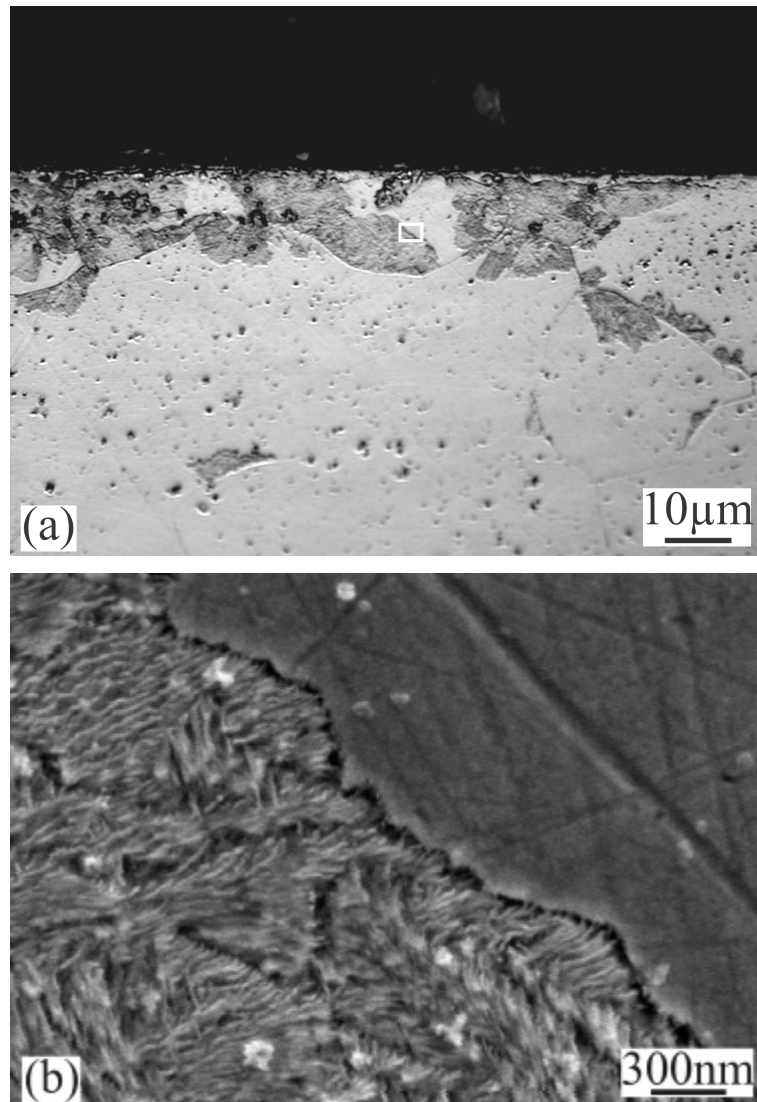
Fig. 2.2: (a) Light micrograph of the surface region of the Fe-4Cr sample nitrided for 19 h at 450 °C. (b) SEM micrograph of the region indicated in (a).

In the Fe-4Cr sample nitrided for 55 h the brighter grains, which do not show discontinuous precipitation, have an average hardness value (1293 HV) higher than measured for the darker grains with the lamellar morphology (898 HV). This suggests that in the bright grains continuous precipitation of chromium nitride as small, finely dispersed precipitates had occurred (invisible by light microscopy). The hardness values of the Fe-4Cr alloy nitrided for 19 h range from 670 to 490 HV towards the middle of the cross-section because the sample was not completely through nitrided (see results of EPMA shown in Fig. 2.3a). The Fe-7Cr alloy has an average hardness of 654 HV. It is not possible to distinguish between hardness values measured for discontinuously precipitated areas and for not discontinuously

precipitated areas because, as mentioned above, almost every grain contains discontinuously transformed areas.
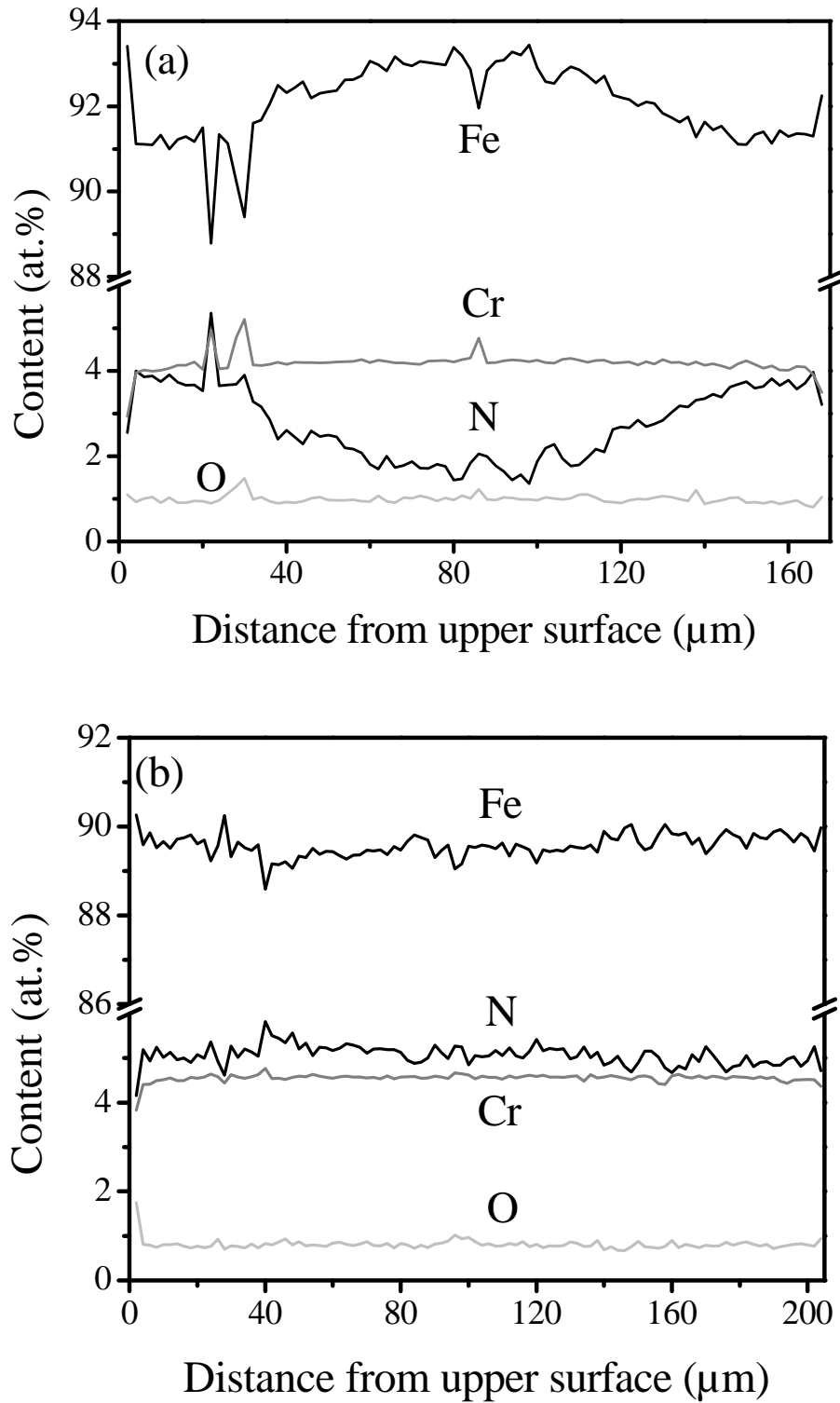

Fig. 2.3: Results of EPMA line scans across the cross-sections of the Fe-4Cr sample nitrided at 450 °C for (a) 19 h and (b) 55 h.

The Fe-4Cr sample nitrided for 55 h has been completely through nitrided, as confirmed by the results of the EPMA measurements. The Fe, Cr, N and O contents of the Fe-4Cr sample (nitrided for 55 h) are shown in Fig. 2.3b. A constant N content which is slightly larger than the Cr content is observed (5.1 at.% N and 4.5 at.% Cr). No difference in composition can be detected between the discontinuously and continuously precipitated regions observed in the optical micrographs. Some local enrichments of Cr and N have been observed by EPMA (visible in Fig. 2.3a for the not through nitrided specimen). This effect is more pronounced after nitriding at 700 °C (see Fig. 2.11).

The X-ray diffractograms measured at the surface show only the presence of α-Fe and Cr_2O_3. Cr_2O_3 is probably only present at the surface (as revealed by XRD after removal of surface material by polishing; see Section 2.3.3). No CrN diffraction peaks can be observed. Apparently, after nitriding at 450 °C, most of the CrN precipitates are coherent with the α-Fe matrix and may diffract coherently with the matrix and/or are too small to yield detectable diffraction peaks.

2.3.2 Nitriding of Fe-4Cr and Fe-7Cr at 580 °C

Cross-sections of the Fe-4Cr and FeCr7 samples nitrided at 580 °C are presented in Fig. 2.4. Features of the morphology obtained after nitriding at 580 °C are similar to those observed after nitriding at 450 °C for both alloys.
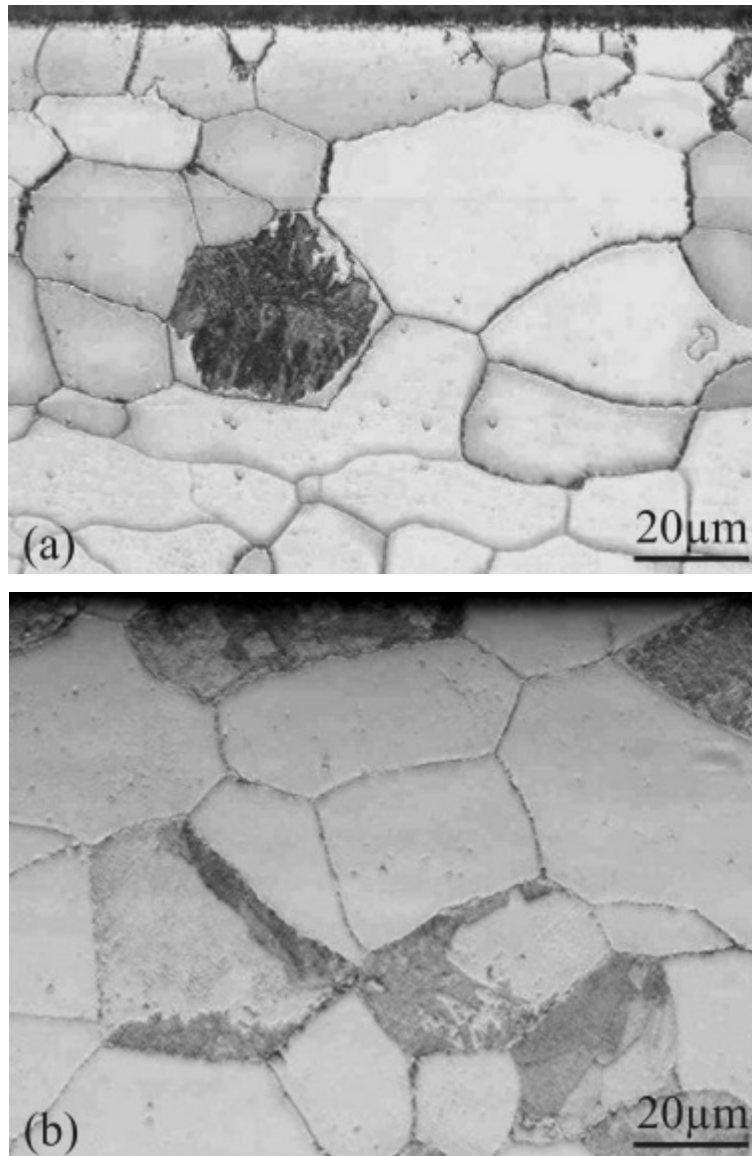

Fig. 2.4: Light micrographs of the Fe-4Cr (a) and Fe-7Cr (b) samples nitrided at 580 °C.

However, in contrast to the alloys nitrided at 450 °C, discontinuously transformed grains appear only isolated and are distributed randomly over the whole sample and thus do not occur preferentially near the surfaces of the specimens. The Fe-7Cr alloy has a clearly higher content of discontinuously precipitated grains than the Fe-4Cr alloy. The transformed grains appear to consist of several discontinuously transformed regions. An enlargement of a grain

partly transformed by the discontinuous precipitation reaction is shown in Fig. 2.5b. Apparent differences in morphology can be caused by orientation differences of the lamellae.
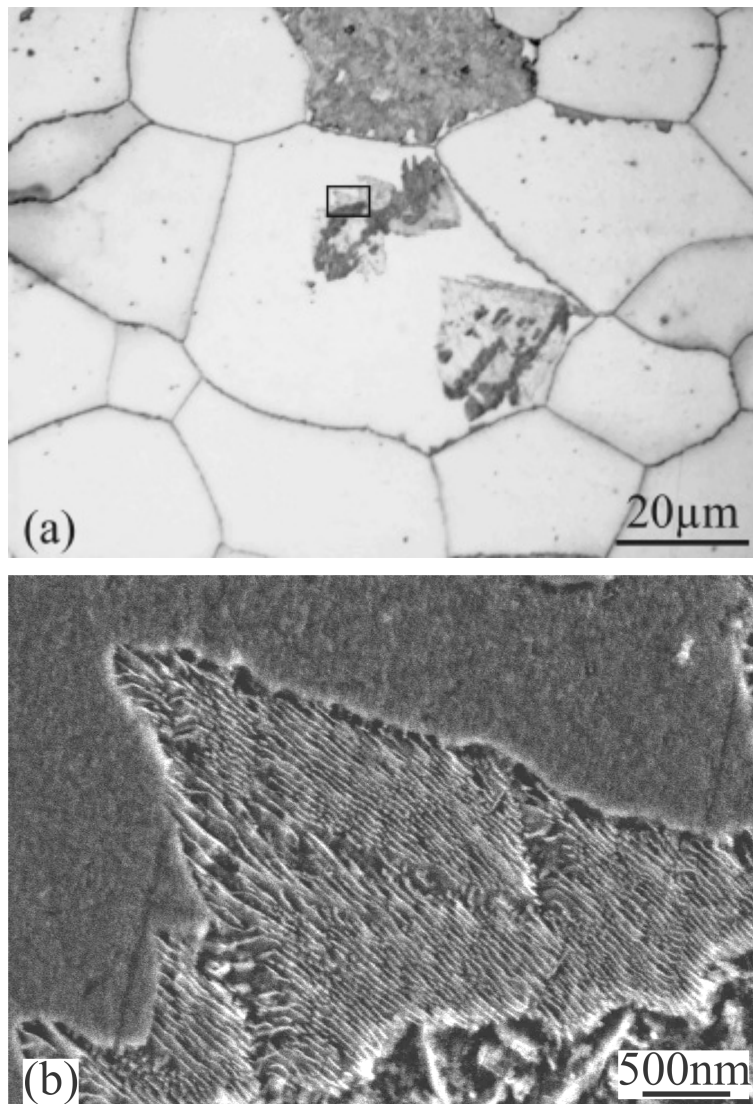

Fig. 2.5: (a) Light micrograph of the Fe-4Cr alloy nitrided at 580 °C. b) SEM micrograph of the region indicated in (a).

Regions with relatively fine lamellae can be recognised as the brighter areas of the discontinuously transformed grains in the light micrograph (Fig. 2.5a). The inter lamellar spacing ranges from 33 to 60 nm.

The measured hardness values of the Fe-4Cr alloy nitrided at 580 °C are similar to those measured near the specimen surface of the Fe-4Cr alloy nitrided at 450 °C for 19 h. Relatively high hardness values (average: 669 HV) were measured in the not transformed areas, which is consistent with the presence of finely dispersed, small CrN precipitates, and relatively low, values (average: 474 HV) were measured in the transformed regions containing CrN and α-Fe

lamellae. The corresponding average hardness values of the Fe-7Cr alloy are 721 HV for the not transformed and 564 HV for the grains transformed by the discontinuous precipitation reaction.

A homogenous distribution of N and Cr is present over the whole sample, as observed for the samples nitrided at 450 °C and as determined by EPMA (average values of 4.7 at.% N for the Fe-4Cr specimen and 8.5 at.% N for the Fe-7Cr specimen).

The X-ray diffractograms show only reflections of α-Fe and Cr_2O_3. After removing surface material by polishing only diffraction peaks of α-Fe are present, proving that Cr_2O_3 is only present at the surface.

2.3.3 Nitriding at 700 °C

2.3.3.1 Fe-4Cr and Fe-7Cr
The specimens nitrided at 700 °C show a precipitation morphology different from that observed for the specimens nitrided at 450 and 580 °C and discussed above. Light and scanning electron micrographs of the Fe-4Cr and Fe-7Cr samples nitrided at 700 °C are shown in Figs. 2.6 and 2.7. The light micrographs suggest that the samples have been transformed completely.
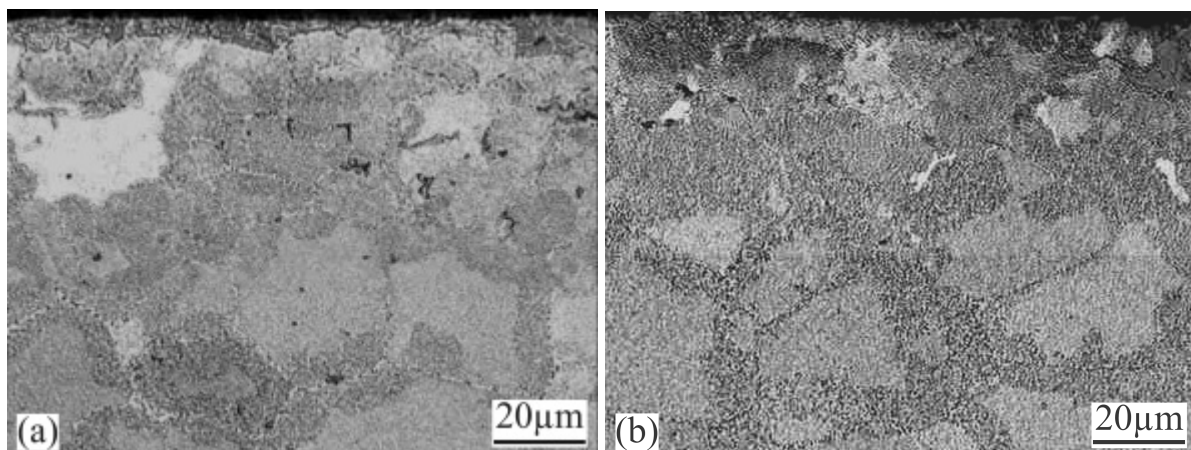
Fig. 2.6: Light micrographs of the Fe-4Cr (a) and Fe-7Cr (b) samples nitrided at 700 °C.

A difference in etching effect of the centre of the grains and of the region near the grain boundaries can be observed, which hints at a difference in precipitation morphology for these regions. The SEM micrographs do not show the presence of lamellae-like structures, as typical for discontinuous precipitation reaction (cf. Figs. 2.2b and 2.5b). Instead, SEM analysis reveals a morphology composed of small particles in a matrix (see Fig. 2.7). The

difference in appearance between the grain centre and the grain boundary regions as observed with light microscopy (Fig. 2.6) can slightly be recognised in the SEM micrographs (Fig. 2.7).
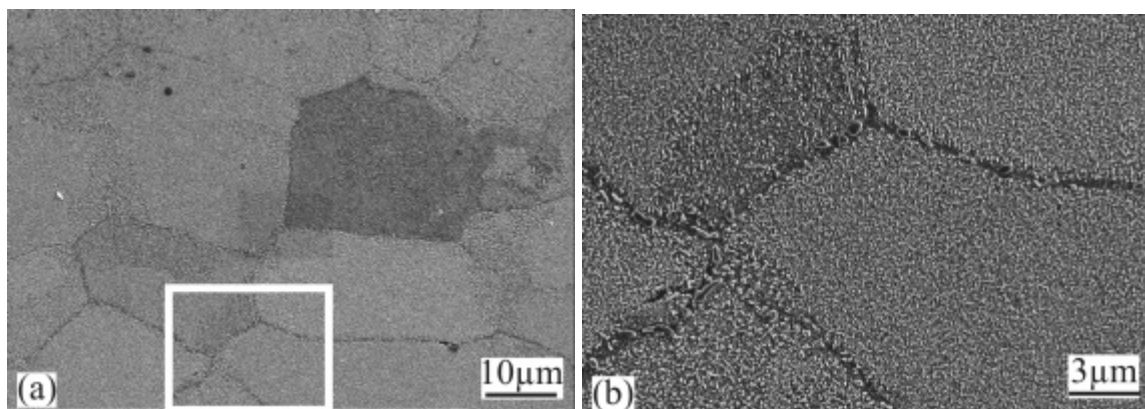

Fig. 2.7: SEM micrographs of the Fe-4Cr sample nitrided at 700 °C. (b) is the enlarged area in (a).

The SEM micrographs show that these differences have their origin in a different particle size: near and at the grain boundaries larger particles occur. Further, the grain boundaries, particularly near the sample surface, show generally (Fig. 2.8) an "open" morphology, i.e., along these grain boundaries a series of pores can be observed. Pores are also observed occasionally within the grains (Fig. 2.8). The presence of pores is also observed after nitriding at 450 and 580 °C, but they occur in particular in specimens that were nitrided at 700 °C. It was confirmed that these pores did not form during the etching process but during nitriding because they are already visible in the as polished condition (cf. Fig. 2.8).
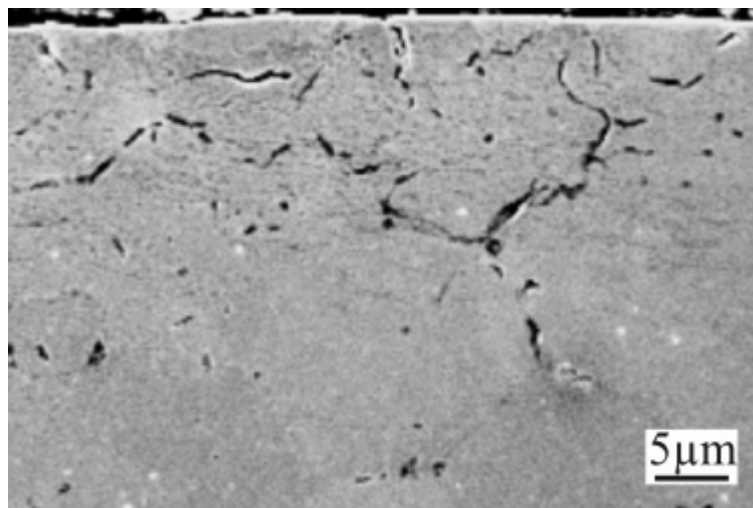

Fig. 2.8: SEM micrograph of the as-polished (not etched) Fe-4Cr sample nitrided at 700 °C, showing pores and cracks in the surface region.

The hardness measurements for the specimens nitrided at 700 °C yielded lower hardness values than those measured for the samples nitrided at 450 and 580 °C. The average hardness value in the centre of the grains is 403 HV for Fe-4Cr and 508 HV for Fe-7Cr; the average hardness value near the grain boundaries is 291 HV for Fe-4Cr and 293 HV for Fe-7Cr. The lower hardness near the grain boundaries is consistent with the coarser precipitation morphology in these areas.

The EPMA shows again a constant N content throughout the specimen (average value of 4.9 at.% N for the Fe-4Cr specimen and 7.4 at.% N for the Fe-7Cr specimen). For the specimen nitrided at 700 °C the EPMA analyses also often show a local enrichment of Cr and N (and a corresponding decrease of the Fe content) near pores and, therefore, especially near grain boundaries (see Fig. 2.12 for Fe-13Cr).
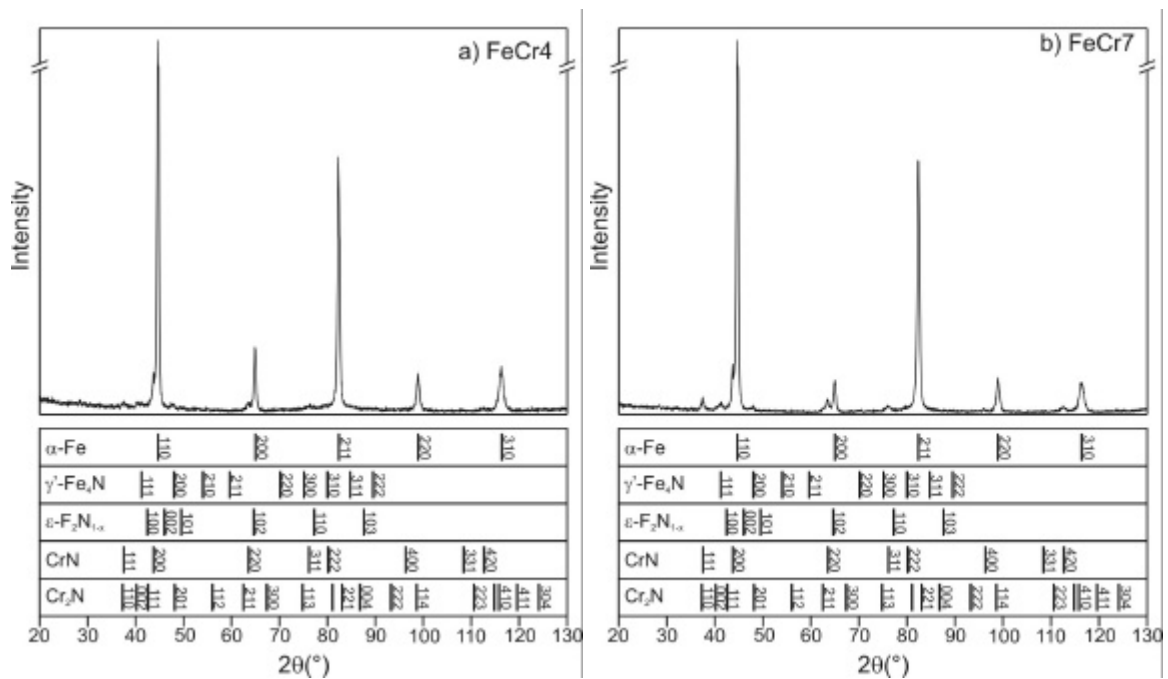
*Fig. 2.9: X*RD diffractograms of the Fe-4Cr (a) and Fe-7Cr (b) alloys nitrided at 700 °C.

The X-ray diffractograms recorded from the surface of the specimens show the presence of Cr_2O_3, γ'-Fe_4N, CrN, and α-Fe. After removing surface material by polishing diffraction peaks of α-Fe, γ'-Fe_4N, and CrN are present in the diffractogram of both samples (see Fig. 2.9); hence again, Cr_2O_3 occurs only at the surface of the specimen. The occurrence of CrN diffraction peaks is consistent with the presence of relatively coarse CrN particles (cf. discussion at the end of Section 2.3.1).

2.3.3.2 Fe-13Cr and Fe-20Cr

The Fe-13Cr and Fe-20Cr alloys nitrided at 700 °C show a relatively homogenous morphology. Light micrographs of the Fe-13Cr sample, (see Fig. 2.10a) show a different etching effect for the regions near the grain boundaries and the centre of the grains, as also observed for Fe-4Cr and Fe-7Cr (see above). However, the grain boundary region is smaller than for the Fe-4Cr and Fe-7Cr specimens (cf. Fig. 2.6). In the light micrographs of the Fe-20Cr specimen (Fig. 2.10b) a different etching of grain centre and boundary region is hardly visible.

Both alloys, but particularly Fe-20Cr, show many "open" grain boundaries. Contrary to the Fe-4Cr and Fe-7Cr alloys nitrided at 700 °C, "open" grain boundaries and pores are not only present near the specimen surface but they occur across the entire specimen cross section. The hardness values measured are similar to those measured for the Fe-4Cr and Fe-7Cr specimen nitrided at 700 °C. The average values for the Fe-13Cr specimen are 510 HV in the middle of the grain and 298 HV in the region near the grain boundaries. The average hardness of the Fe-20Cr specimen is 464 HV. Characteristic of the Fe-13Cr and Fe-20Cr alloys nitrided at 700 °C is their brittleness. Cracks can be observed along the grain boundaries of the Fe-13Cr and Fe-20Cr alloys (see arrows in Fig. 2.10a).
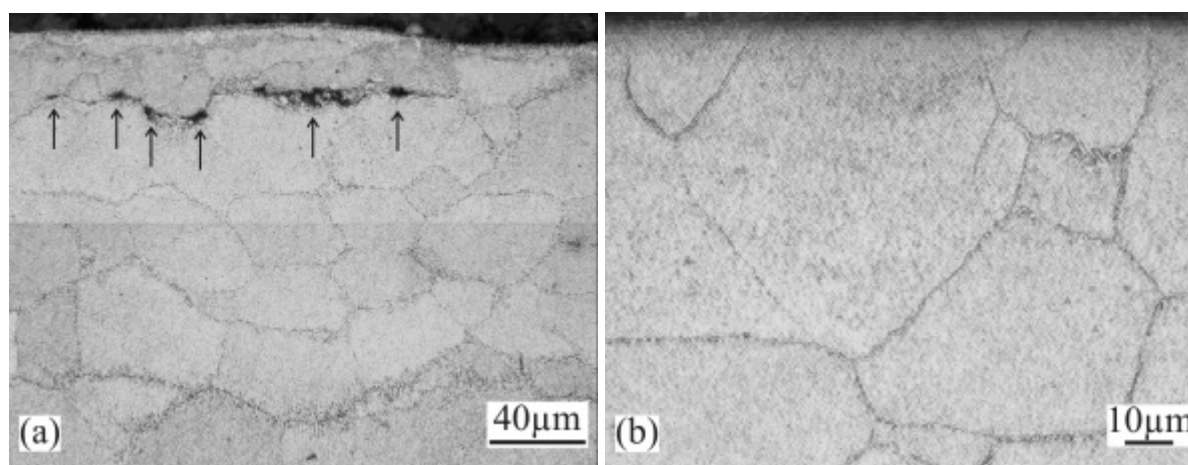
Fig. 2.10: Light micrographs of the Fe-13Cr (a) and Fe-20Cr (b) alloys nitrided at 700 °C

The results of EPMA (see Fig. 2.11 for Fe-13Cr) show again an overall homogenous nitrogen content, slightly larger than the Cr content (average values are 14.6 at.% N for the Fe-13Cr specimen and 20.2 at.% N for the Fe-20Cr specimen). As can be clearly seen in Fig. 2.11, at some positions evident deviations of the overall composition occur: generally, an

increase of the Cr and N content is associated with a decrease of the Fe content. Sometimes also a slightly higher O content could be observed at the same locations. These deviations are observed for all nitrided alloys, but they occur especially in alloys which contain higher Cr contents and which have been nitrided at 700°C. The variations in composition occur mainly at and near pores and "open" grain boundaries. This is for example illustrated by the EPMA intensity map shown in Fig. 2.13.
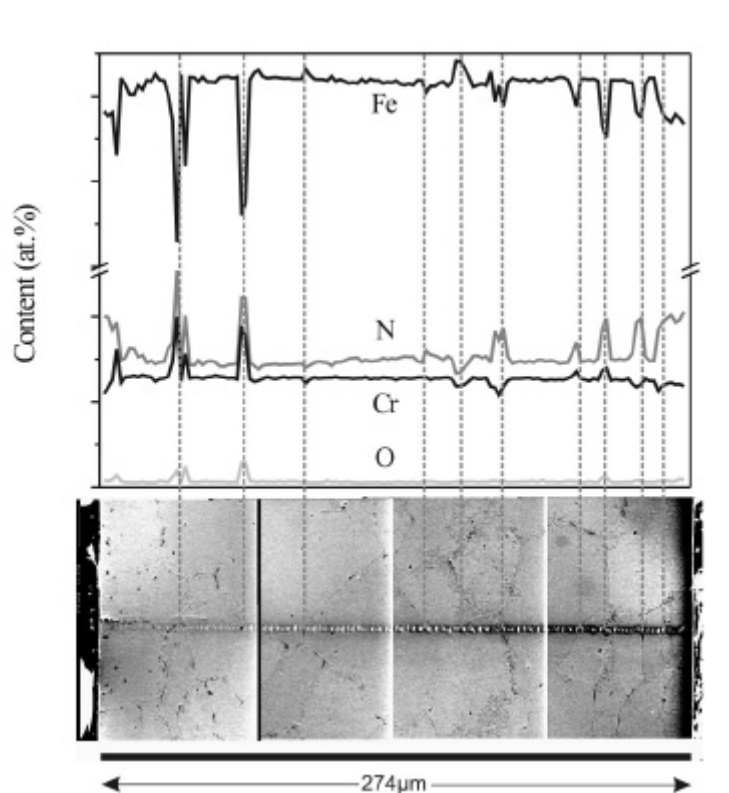
Fig. 2.11: Results of the EPMA line-scan and the corresponding SEM micrograph of the cross-section of the Fe-13Cr alloy nitrided at 700 °C. The vertical dashed lines mark the positions of grain boundaries and pores.

To investigate these concentration variations on a smaller spatial scale than is possible with EPMA, AES measurements of the Fe-13Cr specimen nitrided at 700 °C were made. The Fe LMM, Cr LMM, N KLL, C KLL and O KLL spectra were measured along lines across grain boundaries and pores. The corresponding intensities (peak-to-peak height of the differentiated spectra) near a pore are presented in Fig. 2.14. Evidently, the AES measurements show an increase of Cr and N and sometimes O, and a decrease of Fe near and at the pore shown in Fig. 2.14.

The XRD measurements for both alloys show again the presence of Cr_2O_3, γ'-Fe_4N, CrN and α-Fe at the surface. After removing surface material by polishing only diffraction peaks

of α-Fe, γ'-Fe$_4$N, and CrN are present in the diffractograms of the Fe-13Cr and Fe-20Cr specimens (see Fig. 2.14), indicating again that Cr$_2$O$_3$ only occurs at the surface of the specimens.

2.4 Discussion

2.4.1 Nitriding high chromium – alloyed steels

The measurements have shown that during nitriding nitrogen diffuses into the Fe-Cr alloys and, due to the relatively strong N-Cr interaction, bonds with Cr to form CrN. Apparently, the presence of a Cr$_2$O$_3$ oxide layer at the surface does not impede the nitrogen uptake. At 700 °C in all Fe-Cr alloys investigated (i.e., up to 20 wt. % Cr) CrN has been formed. Recent experiments in another, new nitriding furnace developed by our group show that it is possible to nitride Fe-20Cr at temperatures even as low as 380 °C. Especially for the alloys with a high Cr content, a Cr$_2$O$_3$ layer is present on the sample surface before nitriding. For this reason, in nitriding practice it is said that steels of high Cr content cannot be nitrided. The present work shows that this opinion needs modification. Light micrographs of nitrided Fe-20Cr alloys, which were taken from samples nitrided for a short time (5 h) at 580 °C show that growth of the nitrided zone initiates at a few locations at the sample surface [chapter 3 or 22]. It may be assumed that at these sites the Cr$_2$O$_3$ layer shows some pores or cracks. Such development of cracks in the oxide layer could be explained as a consequence of the difference in thermal expansion coefficient of the oxide layer and of the substrate: upon heating up of the specimens in the nitriding furnace in a protective gas atmosphere, as is the case here (cf. Section 2.2.2), cracks and pores can develop in the oxide layer. On this basis the impossibility to nitride high Cr alloyed steels in practice can be understood: heating up of the workpieces to the nitriding temperature occurs in an atmosphere containing some oxygen as well and thus the substrate under the developing cracks is immediately oxidized again.

2.4.2 Precipitation morphology

Initially the chromium nitride is formed as finely dispersed precipitates, which are probably coherent with the α-Fe matrix [4, 17, 23]. The misfit-induced stress fields associated with these precipitates cause relatively high hardness values. On prolonged nitriding a coarsening of the CrN precipitates occurs, driven by the reduction of the Gibbs energy as a result of relaxation of the internal stress field (and of the precipitate/matrix interfacial area), which is

accompanied with a decrease of the hardness [16, 17]. This coarsening can occur as a continuous transformation, i.e., a gradual increase of the size and decrease of the number of precipitates, or it can take place as a discontinuous transformation, where generally lamellae grow from nucleation sites (surfaces, grain boundaries) into the grains. Thus, upon nitriding of Fe-Cr alloys two reaction fronts can be expected, the first one is due to inward diffusion of nitrogen and the reaction of Cr and N to finely dispersed CrN precipitates, and the second one is due to the subsequent coarsening of the precipitates. The resulting depth dependent morphology of the specimen depends on the nitriding conditions (temperature, nitriding potential, time) and the specimen conditions (composition, grain size, deformation, surface state).

2.4.2.1 Nitriding at 450 and 580 °C
The Fe-4Cr and Fe-7Cr alloys that were nitrided at 450 and 580 °C contain grains with a relatively high hardness (the bright grains in the light micrographs: Figs. 2.1 and 2.4) and grains with a relatively low hardness (the dark grains in Figs. 2.1 and 2.4). The relatively high hardness values correspond with the presence of finely dispersed, coherent (or semi coherent), small CrN precipitates. The SEM micrographs of the grains with the lower hardness value show that a lamellae-like structure is present in these grains (Figs. 2.2 and 2.5). Thus, the coarsening of the CrN precipitates in these grains has occurred as a discontinuous transformation reaction:

$$\alpha' + \beta' \rightarrow \alpha + \beta \tag{1}$$

where β' denotes coherent CrN precipitates in a supersaturated matrix α'. The reaction consists of the replacement of coherent CrN precipitates by CrN lamella $\beta' \rightarrow \beta$ under simultaneous elimination of the supersaturation of the matrix $\alpha' \rightarrow \alpha$ [17].

In the Fe-4Cr alloys which were nitrided at 450 °C the transformed grains occur mainly near the specimen surface, implying that the discontinuous transformation reaction has started mainly in grains near the surface. Similar observations have been reported before [17, 24]. The Fe-4Cr sample that was nitrided for 55 h shows also in the middle of the specimen a relatively high content of grains that had experienced the discontinuous precipitation reaction. In the Fe-7Cr alloy nitrided at 450 °C the discontinuous precipitation has occurred in almost every grain. The discontinuous precipitation reaction initiates at grain boundaries. Thus the morphological difference between the nitrided Fe-4Cr and Fe-7Cr alloys can be interpreted such that the grain boundaries in the Fe-7Cr alloys offer more nucleation sites for the

discontinuous precipitation reactions perhaps because of the presence of a relatively high amount of segregated Cr (and possibly N, upon nitriding). Suitable nucleation sites are not always available at grain boundaries. Indeed, single grains at the specimen surface have been observed which exhibited no discontinuous precipitation although CrN precipitates had formed in a relatively early stage of nitriding, as also confirmed by high hardness values measured for such not transformed grains.

Contrary to the specimens nitrided at 450 °C, in the specimens nitrided at 580 °C discontinuously transformed grains could be observed only occasionally and these are not preferentially near the surface, but randomly distributed over the whole sample. In principle the discontinuous transformation of the finely dispersed CrN precipitates (β') in to CrN lamellae (β) can occur only at locations where the CrN precipitates (β') have been formed first. Indeed, for the Fe-4Cr alloys nitrided at 450 °C, discontinuously transformed grains occur in the surface region already before the centre of the specimen has completely been nitrided (cf. Figs. 2.1a and 2.3a). It might be that at 580 °C the inward diffusion of nitrogen is that fast as compared to 450 °C, that when discontinuous precipitation starts finely dispersed CrN precipitates have already been formed throughout the specimen some time. In that case the formation of CrN lamellae might start at any location and not preferably at the surface.

The CrN precipitates that develop upon nitriding at a more elevated temperature will become coarser than those developing at a lower temperature. Consequently, the driving force for the discontinuous precipitation reaction (cf. Eq. (1)) at 580°C will be smaller than at 450 °C. This can explain that less grains have experienced the discontinuous precipitation reaction at 580 °C, as compared to 450 °C (see also the discussion of the morphology developing at 700 °C below).

2.4.2.2 Nitriding at 700 °C
The Fe-Cr alloys nitrided at 700 °C show a completely different morphology as compared to the alloys nitrided at 450 and 580 °C. No lamellar microstructure could be detected with SEM. Instead, more or less globular, relatively coarse precipitate particles occur in the nitrided grains. The Fe-4Cr, Fe-7Cr and partly the Fe-13Cr alloy show a region adjacent to the grain boundaries with a slightly different appearance. These regions contain coarser precipitate particles and have a lower hardness value than the rest of the grain. Generally, the alloys nitrided at 700 °C have lower hardness values than the alloys nitrided at the lower temperatures, which corresponds with the coarser precipitation morphology. This

interpretation is also supported by the presence of clear CrN reflections in the X-ray diffractograms (Fig. 2.12) recorded from the specimens nitrided at 700 °C, which have not been observed for the samples nitrided at 450 and 580 °C.

The origin of the morphology that develops during nitriding at 700 °C may be explained as follows. Initially, the morphology develops similarly as described above for the lower temperatures, i.e., the formation of homogeneously distributed, finely dispersed, relatively small CrN precipitates. However, before the onset of discontinuous transformation at the grain boundaries, at 700 °C a (competitive) coarsening occurs of the initial CrN precipitates. At this relatively high temperature the distances to be covered by Cr diffusion for the continuous growth of the precipitates are not a large limitation. Thus globular, incoherent precipitates can develop. Thereby the driving force for the discontinuous precipitation reaction has become negligible.

With reference to the above discussion the regions at/near the grain boundaries exhibiting (even) coarser precipitated particles, may be a consequence of relatively fast diffusion of Cr along the grain boundaries and thus in particular there facilitating the coarsening reaction.
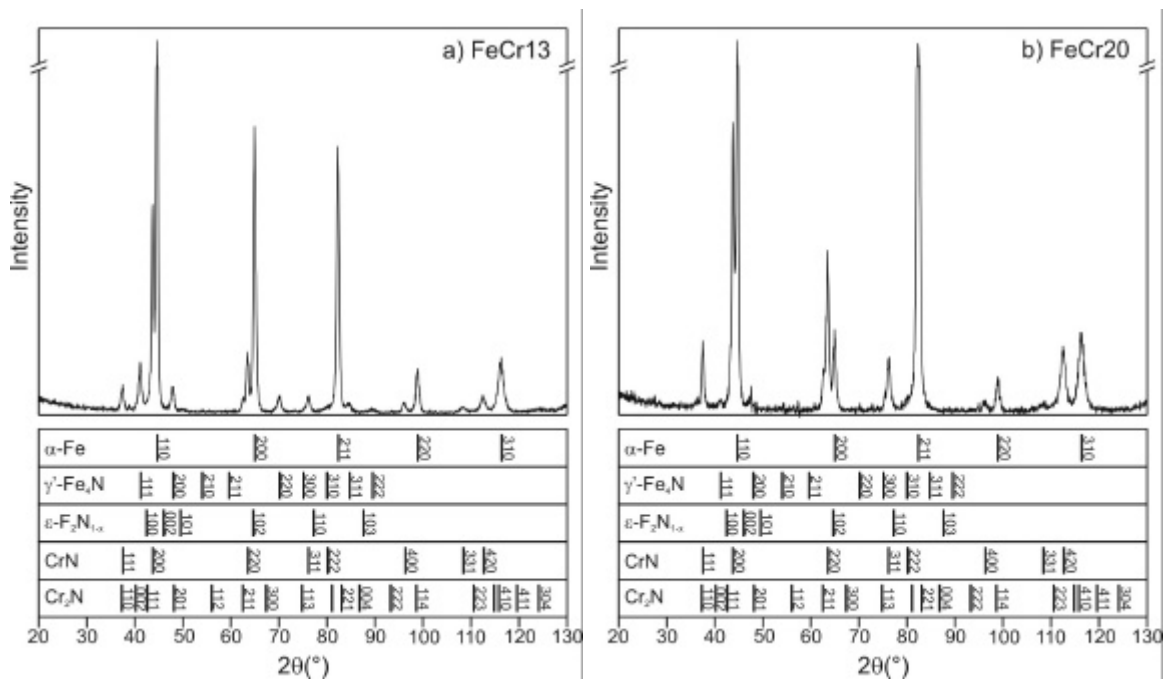

Fig. 2.12: XRD diffractograms of the Fe-13Cr (a) and Fe-20Cr (b) alloys nitrided at 700 °C.

2.4.3 Excess nitrogen

All EPMA measurements performed in this work for all nitrided samples indicate a N atomic concentration that is slightly higher than the Cr atomic concentration. Development of stoichiometric CrN obviously requires equal amounts of atoms Cr and atoms N. The N atomic

concentration can in any case be a little larger than the Cr atomic concentration due to the dissolution of N in the α-Fe matrix. However, this does not completely account for the difference between the N and Cr atomic concentrations (the maximum solubility of nitrogen in ferrite is only 0.4 at.% at 592 °C [7, 17]). For example, for the Fe-4Cr specimen nitrided at 580 °C this means that the maximum nitrogen content would be 0.4 at.% + 4 at.%= 4.4 at.%. The average measured nitrogen content in this sample is 4.8 at.%. The difference (in the example of 0.4 at. % N) between the total amount of N taken up (measured N content) and the sum of the amount of N for precipitation of all Cr as CrN and for equilibrium dissolution of N in the α-Fe matrix (theoretical amount of N) is called excess N.

The excess N can be ascribed to increased lattice solubility of N due to the dilatation of the Fe matrix by the misfit strain fields associated with the coherent CrN precipitates and/or the adsorption of N at the interfaces between the coherent precipitates and the matrix [17,23]. Quantitative analysis of the excess N occurring in the specimens is performed else [22].

2.4.4 Local chromium and nitrogen enrichment at pores and grain boundaries

In many EPMA line-scans local variations of the elemental concentrations, with respect to the average level, can be observed (see Fig. 2.11). This is especially the case for the alloys which were nitrided at 700 °C. The location of these variations is correlated with the presence of pores at grain boundaries and within grains (see Fig. 2.13). Generally, an increase of the N, the Cr, and sometimes the O content, and a decrease of the Fe content is observed. Occasionally, a decrease of the Cr and N content and an increase of the Fe content is observed.

The development of pores is ascribed to the coarsening of the CrN precipitates (especially for the specimen nitrided at 700 °C) and the occurrence of the discontinuous precipitation reaction (especially for the alloys nitrided at 450 and 580 °C). This coarsening of the initial CrN particles and the discontinuous precipitation reaction both lead to incoherent CrN precipitates and a relaxation of the precipitate misfit-strain fields. Thereby, the ability to accommodate excess N becomes reduced or even is lost (see discussion in Section 2.4.3). Then, the excess N can diffuse to grain boundaries (or other large defects) and "precipitate" there as N_2 gas. The correlation between the presence of pores and the increased Cr and N contents suggests that the N_2 gas preferably develops near relatively large CrN precipitates. These large CrN precipitates could preferentially nucleate at chromium oxide impurities (see Fig. 2.13). At the few locations where the measured Cr and N contents are lower and the Fe

content is higher than the average levels, the CrN precipitates have probably been removed during specimen preparation for microstructural analysis.
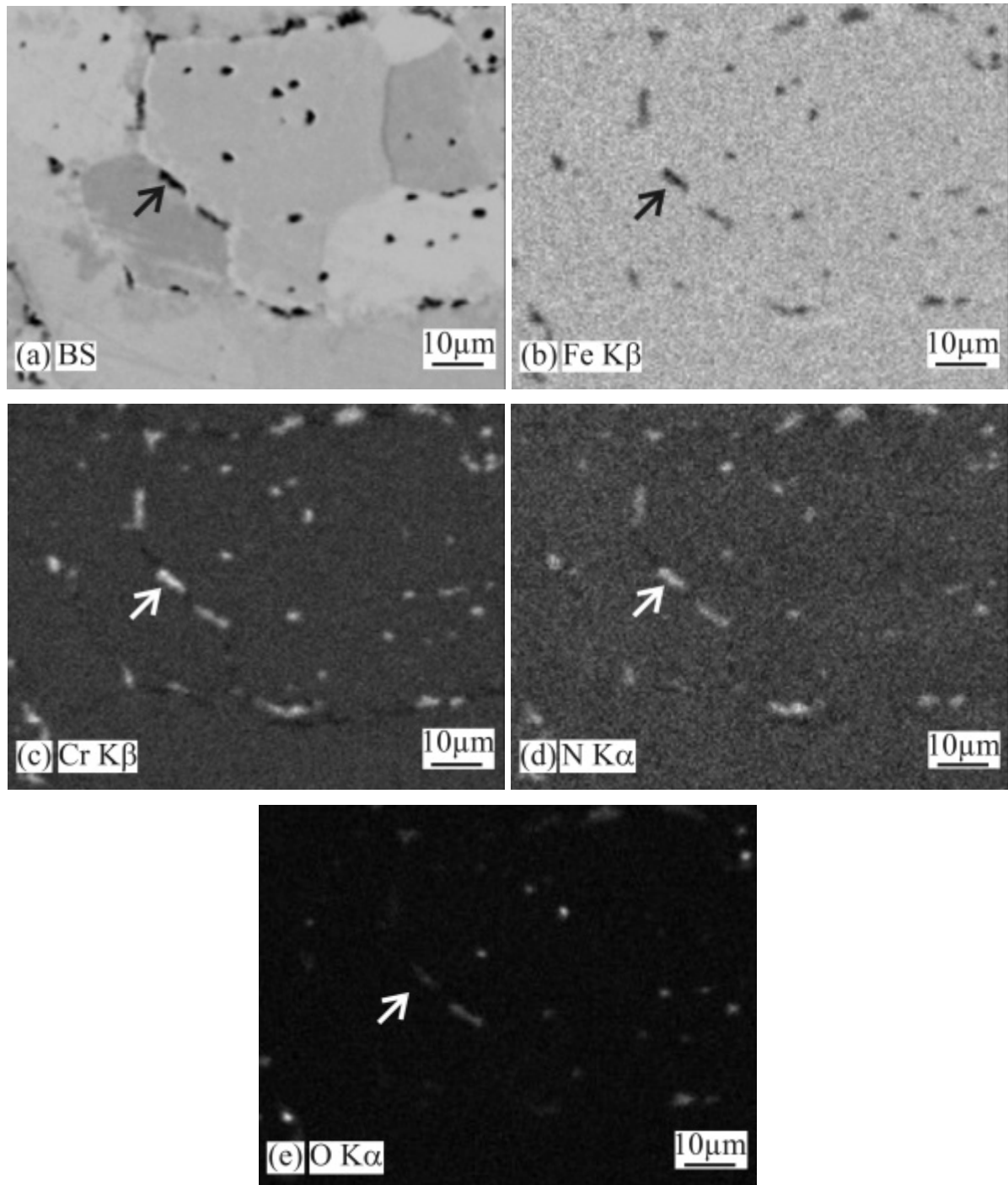

Fig. 2.13: EPMA intensity maps of the Fe-13Cr alloy nitrided at 700 °C. (a) Backscattered electron image, (b) Fe Kβ map, (c) Cr Kβ map, (d) N Kα map, and (e) O Kα map.
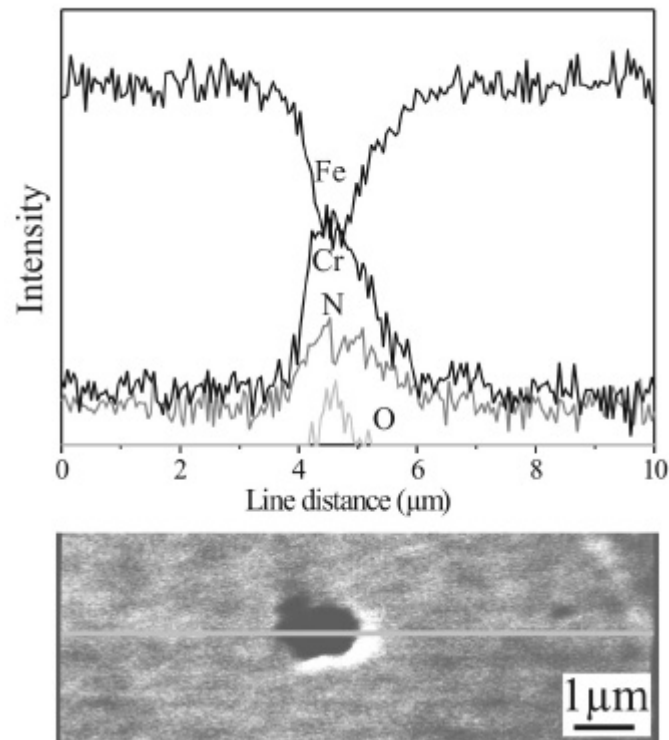
Fig. 2.14: Results of an AES line-scan across a pore of the Fe-13Cr sample nitrided at 700 °C. The line in the SEM micrograph indicates the position of the line-scan.

It should be remarked that EPMA measurements of non-flat sample surfaces, and thus in principle also near pores, generally give wrong composition values. However, in the present case the measured composition deviations are most likely not the result of the local topography, but are genuinly present. This is verified by several observations: (1) If the deviations would be caused by topography the Fe Kβ and Cr Kβ X-ray signals, having approximately the same energy, are expected to have the same deviation in intensity, which is not the case. On the contrary, they have opposite signs and the N Kα signal shows the same deviation as the Cr Kβ signal. (2) The sum of the Fe, Cr, N and O contents is close to 100 % at all locations. (3) The same deviations have been observed in this work employing AES (see Fig. 2.14), a technique with a completely different information volume.

2.5 Conclusions

(i)   Nitriding of ferritic Fe-Cr alloys of high Cr content (20 wt.%) is possible, even at temperatures as low as 380 °C, in contrast with existing experience in the practice of gaseous nitriding. This desired result is ascribed to the development of cracks in the initially present, nitriding inhibiting chromium oxide layer at the surface upon heating to the nitriding temperature in an oxygen-free atmosphere.

(ii) Nitriding at all temperatures investigated (up to 700 °C) leads for all alloys (up to 20 wt.% Cr) to internal precipitation of CrN.

(iii) Upon nitriding at 450 °C first very small, finely dispersed CrN precipitates develop which are coherent with the matrix (no separate precipitate diffraction peaks can be observed). This stage of CrN precipitation is called continuous precipitation. In a second stage of the CrN precipitation process, the very small coherent CrN particles transform by a discontinuous precipitation reaction in an α-Fe/CrN lamellae structure.

(iv) Upon nitriding at 580 °C the same two stages of CrN precipitation occur. However, the number of grains exhibiting the discontinuous precipitation reaction is less than at 450 °C. This is consistent with coarser initial CrN particles, leading to a smaller driving force for the discontinuous precipitation reaction.

(v)   Upon nitriding at 700 °C CrN precipitates occur as coarser particles. Clear CrN diffraction peaks can be observed. At this nitriding temperature distinct Cr diffusion is possible, leading to pronounced coarsening, and thereby rendering the driving force for the discontinuous precipitation reaction to effectively nil: no grains were transformed by the discontinuous precipitation reaction in all alloys nitrided at this nitriding temperature.

(vi) After nitriding all specimens contain more nitrogen than necessary for precipitation of all Cr as CrN and for realisation of the equilibrium dissolution of N in the α-Fe matrix. This excess N is ascribed to (i) enhanced lattice solubility of N due to the precipitate misfit-strain fields and to (ii) adsorption of N at the precipitate/matrix interfaces in the beginning stage of precipitation. The excess N precipitates as N_2 gas causing pores at later stages of the precipitation reaction where the discontinuous precipitation reaction occurs (nitriding at 450 and 580 °C) and/or coarsening of the initial CrN particles becomes appreciable (nitriding at 700 °C). The occurrence of Cr and N enrichment in

the immediate surroundings of the pores suggests that the N_2 gas precipitation in particular is favoured at the interface with large CrN precipitates.

References

[1]   Mittemeijer, E.J. (ed.): Mat. Sci, Forum 102-104 (1992) 223.

[2]   Mittemeijer, E.J.; Slycke, J.T.: Surface Eng. 12 (1996) 152.

[3]   Jack, K.H. in Proc. Conf. on Heat Treatment, The Metals Society, London (1975) 39.

[4]   Mortimer, B.; Grieveson, P.; Jack, K.H.: Scand. J. Metall. 1 (1972) 203.

[5]   Lehrer, E.: Z. Elektrochem. 36 (1930) 383.

[6]   van Wiggen, P.C.; Rozendaal, H.C.F.; Mittemeijer, E.J.: J. Mater. Sci. 20 (1985) 4561.

[7]   Mittemeijer, E.J.; Somers, M.A.J.: Surface Eng. 13 (1997) 483.

[8]   Maldzinsky, L.; Lilienthal, W.; Tymowski, G.; Tacikowski, J.: Surface Eng. 15 (1999) 377.

[9]   Somers, M.A.J.: Heat Treat. Met. 4 (2000) 92.

[10]   Du, H; Ågren, J.: Metall. Mater. Trans. A 27 (1996) 1073.

[11]   Torchane, L.; Bilger, P.; Dulcy, J.; Gantois, M.: Metall. Mater. Trans. A 27 (1996) 1823.

[12]   Du, H.; Ågren, J.: Z. Metallkd. 8 (1995) 522.

[13]   Somers, M. A. J.; Mittemeijer, E.J.: Metall. Mater. Trans. A 26 (1995) 57.

[14]   Du, H.; Lange, N.; Ågren, J.: Surface Eng. 11 (1995) 301.

[15]   Sumin, V.V.; Muzychka, A.Yu.; Chimid, G.; Rashev, Ts.; Sar'ivanov, L.; Fykin, L.E.: Fizika Metall. Metalloved. 87 (1999) 65.

[16]   Mittemeijer, E.J. ; Vogels, A.B.P.; van der Schaaf, P.J.: J. Mater. Sci. 15 (1980) 3129.

[17]   Hekker, P.M.; Rozendaal, H.C.F.; Mittemeijer, E.J.: J. Mater. Sci. 20 (1985) 718.

[18]   Alves, C; de Anchieta Rodrigues, J.; Eduardo Martinelli, A: Mater. Sci. Eng. 279 (2000) 10.

[19]   Lightfoot, B.J.; Jack, D.H.: As Ref. [3], p. 59.

[20]   JCPDS-International Centre for Diffraction Data (1999), PCPDFWIN, Version 202.

[21]   Pouchou, J.L.; Pichoir, F.: La Recherche Aérospatiale no. 1984-3 13.

[22]   Schacherl, R.E.; Graat, P.C.J.; Mittemeijer, E.J.: in preparation.

[23]   Somers, M.A.J.; Lankreijer, R.M.; Mittemeijer, E.J.: Phil. Mag. A 59 (1989) 353.

[24]   Permyakov, V.G.; Belotskii, A.V.; Barabash, R.I.: Metallofizika 42 (1972) 102.

3. Modelling the Nitriding Kinetics of Iron-Chromium Alloys; the role of excess nitrogen

R.E. Schacherl, P.C.J. Graat, E.J. Mittemeijer

Abstract

To investigate the morphology and the growth kinetics of nitrided layers of Fe-Cr alloys, nitriding experiments were performed for alloys with 4, 7, 13 and 20 wt.% Cr. The precipitation morphology of the nitrided samples was investigated with light optical and scanning electron microscopy. The elemental compositional variation was determined with electron probe microanalysis. To describe the evolution of the thickness of the nitrided layers a numerical model was developed that has as important (fit) parameters: the surface nitrogen content, the solubility product of chromium and nitrogen dissolved in the ferrite matrix and a parameter defining the composition of the precipitated chromium nitride. Fitting of the model to the experimental data demonstrated for the first time that mobile and immobile excess nitrogen is present in the nitrided layers and that the mobile excess nitrogen considerably influences the nitriding rate.

3.1 Introduction

Nitriding of iron-based alloys is a process that can lead to pronounced improvement of the fatigue, corrosion and wear properties of workpieces in countless practical applications [1]. To optimize the properties obtained, the growth kinetics of the surface adjacent nitrided zone, i.e. the thickness increase as dependent on the applied nitriding parameters (time, temperature, nitriding potential, specimen composition), has to be known.

If pure iron is nitrided three different Fe-N phases can occur successively [2]: α-Fe [N] (ferrite) with a bcc structure, where the nitrogen is statistically distributed over the octahedral interstitial sites of the bcc Fe–sublattice, the γ'-Fe$_4$N$_{1-x}$ phase based on an fcc Fe sublattice, where the nitrogen atoms are distributed in an ordered way over the octahedral interstitial sites, and the ε-Fe$_2$N$_{1-x}$ phase based on an hcp Fe sublattice, where the nitrogen atoms are distributed over the octahedral interstitial sites in a more or less ordered way. The amount of nitrogen dissolved in iron depends on the nitriding temperature and the chemical potential of nitrogen in the nitriding atmosphere, which in case of gaseous nitriding can be adjusted by varying the composition of the mixture of the ammonia and the hydrogen in the gas phase [3-5]. If the nitriding conditions allow the formation of ε, it will be formed at the surface. As a second layer γ' will be formed below the ε layer. The surface layer containing the γ' and the e phases (sublayers) is called "compound layer". The last "layer", underneath γ', the so-called "diffusion zone", consists of α-Fe (the original substrate) where the nitrogen atoms are dissolved interstitially (see above) [5-9].

If the iron matrix (substrate) contains alloying elements with a relatively high affinity for N, nitrides of these elements can be formed during nitriding and these thus occur in the "diffusion zone". Cr is often used as an alloying element in nitriding steels, because of the relatively strong Cr-N interaction [10-12], which allows the formation of chromium nitride [13, 14]. During the nitriding process the formation of chromium nitride proceeds by nucleation and growth. In the initial stage very small coherent, precipitates develop. This stage is associated with a relatively high hardness, caused by the strain fields, which are induced by the misfit between the CrN particles and the α-Fe matrix [14]. Continued nitriding involves aging for the CrN particles already formed and left behind in the wake of the migrating reaction front. This aging process leads to coarsening of these CrN precipitates, in association with loss of coherency, corresponding with decrease of misfit strain energy and

decrease of a-Fe/CrN interfacial area [14]. The coarsening process can occur as so-called "continuous coarsening" involving growth of larger particles at the cost of smaller particles or as "discontinuous coarsening" (cf. terminology given in Ref.[15]) involving development of a lamellar structure of CrN and α-Fe [14, 16-21]. Both coarsening reactions can occur simultaneously and lead to decrease of hardness which is most pronounced for the lamellar microstructure [14]. A peculiar and important (see what follows) observation is the occurrence of so-called excess nitrogen: enhanced uptake of nitrogen in the nitrided zone, ascribed to the nitride-precipitate / matrix misfit-strain field [12, 14].

Obviously, with a view to practice, model descriptions for the kinetics (i.e. time and temperature dependencies) of (ε/γ') nitride layer growth and diffusion zone growth are needed. A satisfactory approach for modelling (bi)layer (nitride) growth (i.e. compound layer growth) upon nitriding iron exists [5, 6]. For describing the growth of the diffusion zone under simultaneous development of alloying-element nitrides, a satisfactory, generally valid model has not been presented until now (see also discussion in section 3.2). According to the present authors this may be due to the ignorance of the role of the so-called excess nitrogen (cf. above discussion) on nitriding kinetics. This work presents a general model for the description of the nitriding kinetics of iron-based alloys, incorporating the excess nitrogen (section 3.2). The model allows distinction between the effects of "mobile" and "immobile" excess nitrogen and has been applied successfully to Fe-Cr alloys subjected to gaseous nitriding (section 3.4).

3.2 Model for the kinetics of diffusion zone growth

Consider a Fe-Me alloy that is nitrided employing a nitriding potential such that no iron nitrides can be formed at the surface, but upon nitriding a diffusion zone containing MeN_n nitride particles develops.

The first proposals to describe diffusion zone growth upon nitriding have been derived from a simple model originally meant for "internal oxidation" [22]. The following assumptions have to be made for this model, if it is applied to "inner nitriding" [14, 22]:

(i)   The nitrogen dissolved in the ferrite matrix (α) exhibits Henrian behaviour. This implies that the diffusion coefficient of nitrogen in the ferrite matrix is independent of the dissolved nitrogen content.

(ii)   The reaction of dissolved nitrogen with dissolved Me, leading to the nitride MeN_n, takes place only and completely at a sharp interface between the nitrided zone and the not nitrided core.

(iii) The amount of nitrogen which is required for building up the concentration profile in the ferrite matrix of the nitrided zone is negligible in comparison to the amount of nitrogen which is consumed at the reaction interface.

(iv) Diffusion of Me can be neglected and is not nitriding-rate determining.

(v)   Nitrogen is taken up rapidly from the nitriding medium / specimen surface, so that the surface concentration c_N^S is equal to the lattice solubility of nitrogen, corresponding to the chemical potential of nitrogen in the nitriding atmosphere.

With these assumptions and approximating the concentration gradient of dissolved nitrogen with $-c_{N_a}^S/z$ the amount of nitrogen (per unit area) which reaches the reaction front in the time period dt is equal to $\left(c_{N_a}^S \cdot D_N / z\right) dt$, where z is the depth coordinate of the reaction front. This nitrogen amount must equal the nitrogen amount required to move the reaction front a distance dz, i.e.: $n \cdot c_{Me} \cdot dz$, where c_{Me} is the Me concentration. Upon integration of the resulting differential equation for constant temperature it is obtained:

$$z^2 = \left(\frac{2 \cdot c_{N_a}^S \cdot D_N}{n \cdot c_{Me}} \right) \cdot t \qquad\qquad (1)$$

Hence, at constant temperature a parabolic relation should occur between the nitriding time and the thickness of the nitrided layer.

   This model has been often used to predict the case depth of the nitrided zone [14, 17, 23]. A major simplification introduced in applying the model is that the solubility of nitrogen in the ferrite matrix is taken as that pertaining to unstrained, pure α-Fe; excess nitrogen dissolved in the α-Fe matrix is not considered.

   Excess nitrogen is the amount of nitrogen, which exceeds the "normal" capacity of nitrogen uptake. This normal capacity for nitrogen uptake consists in the case of a Fe-Me alloy of:

   −   the amount of nitrogen dissolved interstitially in the unstrained α-Fe matrix and

   −   the amount of nitrogen, which is incorporated in the MeN_n precipitates.

The difference between the total amount of nitrogen in the nitrided zone and this normal capacity is defined as "excess" nitrogen. Three types of "excess" nitrogen are distinguished: (i) nitrogen which is trapped at dislocations (in particular for deformed alloys [24]), (ii) nitrogen which is adsorbed at matrix/precipitate interfaces and (iii) nitrogen which is (additionally) dissolved in the strained α-Fe matrix. Such excess nitrogen was found in nitrided Fe-Ti [25-27], Fe-V [28], Fe-Mo [28], Fe-Al [24, 29] and Fe-Cr alloys [14, 21, 30].

With a view to the nitriding kinetics the effects of the various kinds of excess nitrogen will be different. It is proposed here to distinguish between mobile excess nitrogen, i.e. nitrogen dissolved in the ferrite lattice, and immobile excess nitrogen, i.e. nitrogen trapped at dislocations and adsorbed at the nitride/matrix interfaces. Mobile excess nitrogen will enhance the extent of the diffusion zone, whereas immobile excess nitrogen will decrease the extent of the nitrided zone. This becomes immediately clear, already on inspection of the simple Eq. (1): mobile excess nitrogen expresses itself by an increase of the lattice solubility $c_{N_a}^S$; immobile excess nitrogen may be effectively expressed by an increase of the stoichiometric parameter n. However, to avoid the crude simplifications inherent to application of Eq. (1), in this paper the following numerical model is proposed to incorporate the effects of immobile and mobile excess nitrogen on nitriding kinetics.

The inward diffusion of nitrogen in the α-Fe matrix can be described with Fick's second law:

$$\frac{\partial c_{N_a}(z,t)}{\partial t} = D_N \cdot \frac{\partial^2 c_{N_a}(z,t)}{\partial z^2} \tag{2}$$

$c_{N_a}(z,t)$ is the nitrogen dissolved in the α-Fe matrix at the depth z at time t and at temperature T. D_N is the diffusion coefficient of nitrogen in α-Fe, which can be taken as concentration independent [5, 6]. The formation of nitrides of possibly present alloying elements removes dissolved, mobile nitrogen from the matrix, which nitrogen then is trapped as immobile nitrogen in the nitrides formed. The formation of MeN_n can be expressed with the following equation:

$$Me_a + nN_\alpha \Leftrightarrow MeN_n \tag{3}$$

Where Me_α and N_α denote alloying element and nitrogen dissolved in the α-Fe matrix. The equilibrium constant of the above reaction, K_e, obeys

$$K_e = \frac{1}{[Me_a] \cdot [N]^n} = \frac{1}{K_{MeN_n}} \text{ with } K_{MeN_n} = [Me_a] \cdot [N_a]^n \tag{4}$$

where $[Me_\alpha]$ and $[N_\alpha]$ denote the concentrations of dissolved Me and dissolved N in the α-Fe matrix and K_{MeN_n} is the corresponding solubility product of Me_α and N_α. The precipitation of MeN_n will take place at a certain location if there it holds

$$[Me_\alpha][N_\alpha]^n > K_{MeN_n} \tag{5}$$

In solving Fick's second law (Eq. (2)) it must be tested at every location (depth z) for every time (step) if the solubility product, K_{MeN_n}, is surpassed. If this is the case, precipitation of MeN_n, at the location considered, should be allowed for until $[Me_\alpha][N_\alpha]^n = K_{MeN_n}$. Thereby a numerical finite difference (explicit method) solution method is naturally suggested to solve Fick's second law, subject to the prevailing boundary conditions. Thus, adopting the finite difference approach of Ref. 31, in this work the nitrogen concentration at depth z_i and at time t_{j+1}, $c_{N_a}(i, j+1)$, is calculated from the nitrogen concentrations at the previous time t_j at the depths i-1, i and i+1 according to:

$$c_{N_a}(i, j+1) = c_{N_a}(i, j) + r \cdot \{c_{N_a}(i-1, j) - 2 \cdot c_{N_a}(i, j) + c_{N_a}(i+1, j)\} \tag{6}$$

where $r = D_N(\Delta t/\Delta z^2)$ with Δt and Δz as time and depth steps.

The application of a solubility product constraint as indicated by Eq. (5) was earlier applied to a case of carburizing [32, 33]. Attempts to apply the approach to cases of nitriding until now either ignored entirely the presence and role of excess nitrogen [34] or, erroneously, considered the excess nitrogen dissolved in the ferrite lattice as immobile, i.e. not contributing

to nitrogen diffusion, and ignored the presence of immobile excess nitrogen adsorbed at the nitride–particles/matrix interfaces (see above) [35].
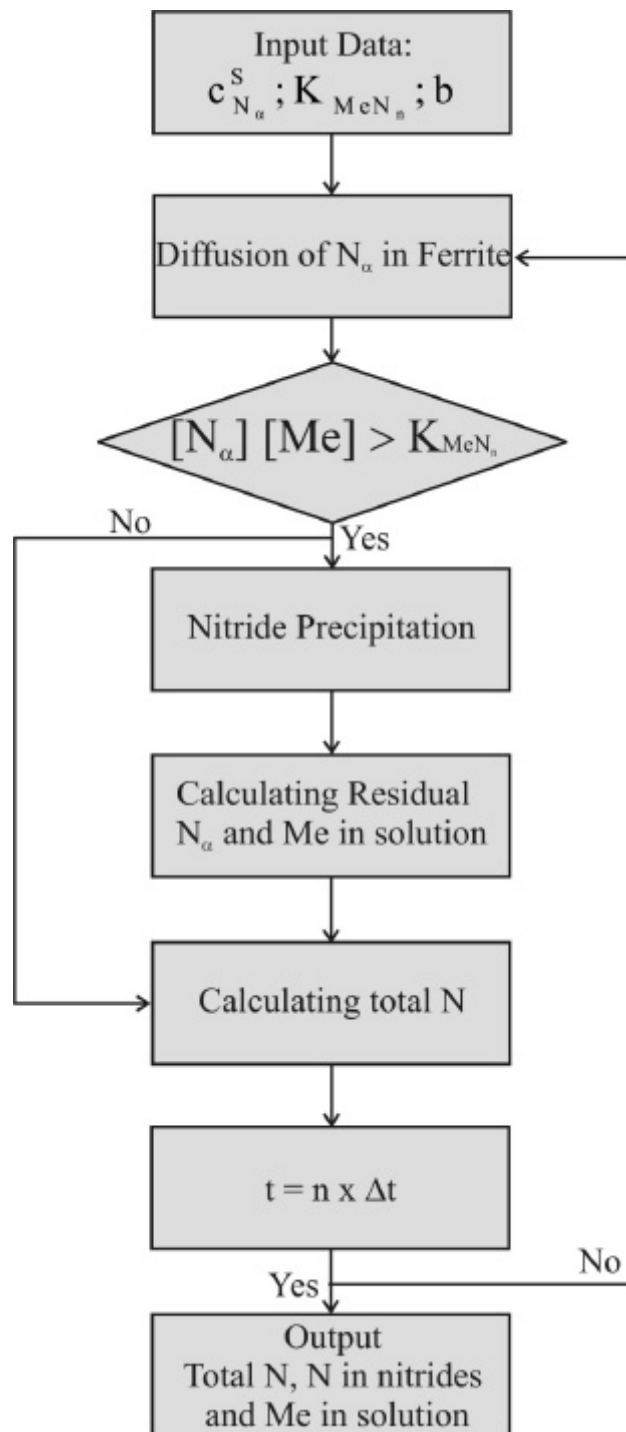

Fig. 3.1: Flow chart showing the scheme of calculating the nitrogen concentration and MeN$_n$ precipitate depth – profiles. Total N denotes the amount of nitrogen bound in CrN and dissolved in the ferrite matrix. The letter n in the flow chart indicates the number of time steps.

In this work the presence of mobile excess nitrogen is recognised by considering the nitrogen lattice solubility at the surface, $c_{N_a}^S$, as a fit parameter (i.e not assume $c_{N_a}^S$ equal to the equilibrium nitrogen solubility of (unstrained) ferrite). The presence of immobile excess nitrogen is recognised by replacing the stoichiometric parameter n in MeN_n by b=n+x, with x as the contribution of the immobile excess nitrogen. The fit parameters in the current model thus are: $c_{N_a}^S$, b and K_{MeN_n}. The scheme of calculating the nitrogen concentration–depth profile, and the depth profile of the amount of MeN_n precipitates, according to the finite difference method, is shown in Fig. 3.1. The following boundary conditions are adopted:

 – The initial nitrogen concentration is constant and given by $c_{N_a}^{t=0}$ (for z≠0): $c_{N_a}(i,1) = c_{N_a}^{t=0}$ for i>1. In the present case $c_{N_a}^{t=0}$ is virtually zero.

 – The surface concentration is always given by $c_{N_a}^S$: $c_{N_a}(1,j) = c_{N_a}^S$.

 – There is no net flux through the centre plane of the specimen (sheet) at $z=z_M$. This is realized by taking the concentrations at the grid points adjacent to the grid point at the centre plane, indicated by i=M, equal to each other, i.e. $c_{N_a}(M-1,j) = c_{N_a}(M+1,j)$. Hence (cf. Eq. (6)):

$$c_{N_a}(M,j+1) = (1-2r)c_{N_a}(M,j) + 2rc_{N_a}(M-1,j) \tag{7}$$

On the above basis the importance of incorporating the presence of both mobile and immobile excess nitrogen in the modelling of nitriding kinetics can be demonstrated by simulations (see what follows).

A Fe-7 wt.% Cr alloy is considered, which is nitrided at 580°C and a nitriding potential of r_n=0.1 atm$^{-1/2}$ for 7h. The solid line in Fig. 3.2 shows the resulting nitrogen-concentration depth profile as calculated for the case that neither mobile nor immobile excess nitrogen is present in the nitrided layer. This means that (i) the surface nitrogen content $c_{N_a}^S$ is equal to the solubility of nitrogen in pure, unstrained ferrite, in accordance with the applied nitriding parameters (r_n=0.1 atm$^{-1/2}$, T=580°C; for data on $c_{N_a}^S$, see Refs. 4, 5) and (ii) that b is equal to n=1 (no immobile excess nitrogen).
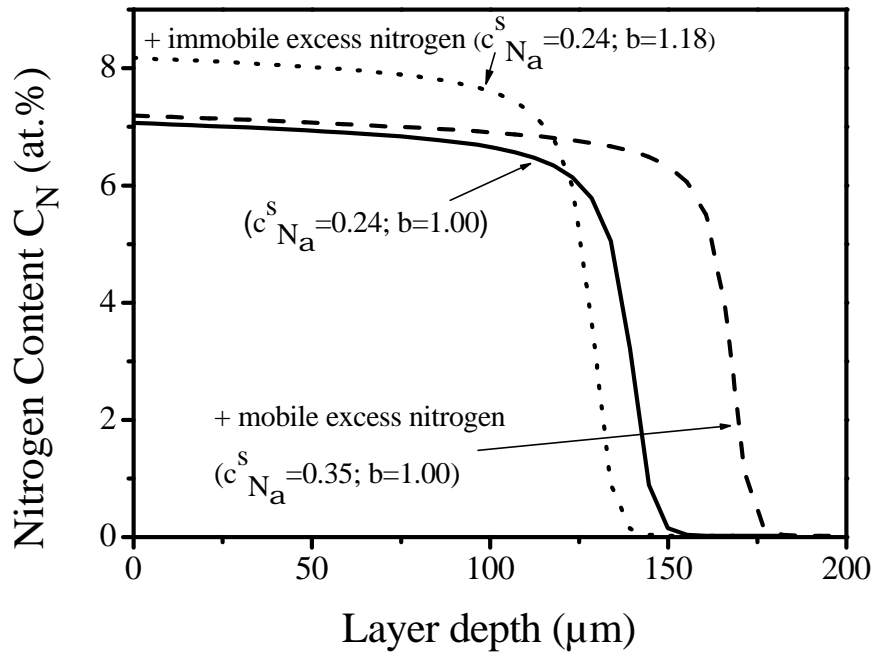
Fig. 3.2: Effect of mobile and immobile excess nitrogen on the development of the nitrogen concentration-depth profile. Fe-7 wt.% Cr alloy sheet nitrided at 580°C at a nitriding potential r_n=0.1 atm$^{-1/2}$.

If only the existence of mobile excess nitrogen is assumed, which is expressed by a higher value for $c_{N_a}^S$, clearly a significantly larger extent (depth) of the nitrided zone occurs (see the dashed line in Fig. 3.2). If only the existence of immobile excess nitrogen is assumed, which is expressed by a value of b larger than n (=1 for the present case of CrN precipitation), a somewhat smaller penetration depth of nitrogen occurs (see the dotted line in Fig. 3.2).

The above used values for $c_{N_a}^S$ and b are realistic values (see section 3.4). Evidently, the presence of mobile and immobile excess nitrogen has a pronounced influence on the nitriding kinetics. The effect of mobile and immobile nitrogen have to be recognised in any model that should be able to predict properties resulting from nitriding.

Another important parameter in the above described numerical model is the equilibrium solubility product, K_{MeN_n}, which controls the (local) occurrence of precipitation. The influence of K_{CrN} on the nitrogen-depth profile is shown in Fig. 3.3.
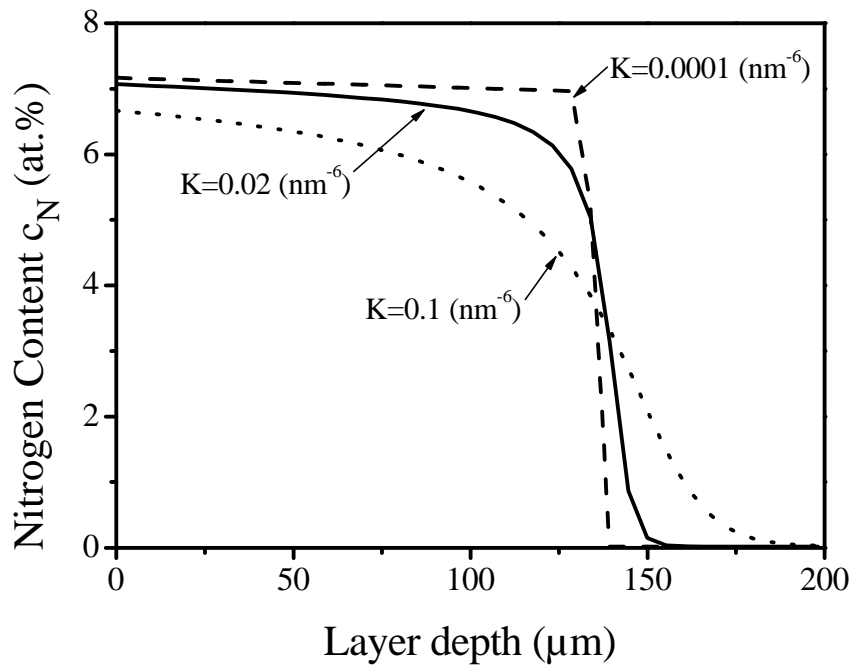
Fig. 3.3: Effect of the solubility product K_{MeN} (nm^{-6}) on the development of the nitrogen concentration-depth profile. Fe-7 wt.% Cr alloy sheet nitrided at 580°C and at a nitriding potential of r_n=0.1 $atm^{-1/2}$ for 7h.

Relatively large K_{CrN} values imply that (at the reaction front) not all dissolved Cr reacts with nitrogen to chromium nitride and thus the extent of the nitrided zone is larger for larger K_{CrN}, although in association with a more gradual transition between the nitrided zone and the not nitrided core of the sample.

3.3 Experimental

3.3.1 Specimen preparation

Fe-Cr alloys with nominally 4, 7, 13 and 20 wt % Cr (coded as Fe-4Cr, Fe-7Cr, Fe-13Cr and Fe-20Cr, respectively) were prepared from pure Fe (99.98 wt.%) and pure Cr (99.999 wt. %) in an inductive furnace under argon atmosphere (99.999 vol. %). The melt process was performed in an Al_2O_3 crucible. The amounts of oxygen, nitrogen, carbon and sulphur impurities in the produced alloys were determined by chemical analysis (inductive-coupled plasma-optic emission spectroscopy). The average results for each alloy composition are shown in Table 1. It is likely that the detected oxygen is thought due to the (natural) oxide layer on the specimen surface.

Table 1: Amounts of light element impurities for each alloy used in this work.

Alloy	O (µg/g):	N (µg/g)	C (µg/g)	S (µg/g)
Fe-4Cr	117 +/- 10	<5	6 +/-2	6 +/-3
Fe-7Cr	132 +/- 10	<5	63 +/- 10	7 +/-3
Fe-13Cr	146 +/- 10	<5	4 +/- 2	5 +/- 2
Fe-20Cr	155 +/- 15	<5	9 +/- 2	3 +/- 2

After casting the alloys have cylindrical shape with a diameter of 10 mm and a length of 100 mm. The cast alloys were cold rolled to sheets with a thickness of 1.2 +/-0.1 mm. The obtained sheets were cut into rectangular pieces of lateral dimensions 1.5x1.5 mm^2. These pieces were subsequently cleaned in an ultrasonic bath filled with ethanol and encapsulated in a silica tube filled with argon (purity: 99.999 vol.%) up to a pressure of 750 Torr. The encapsulated samples were annealed for 1h at 700 °C (within the α-phase region of the Fe-Cr diagram) to get a recrystallized grain structure. After annealing the grains had an average diameter of 45µm.

Electron probe microanalysis (see also section 3.3.3.4) was used to verify that Cr was distributed homogenously in the sample. Before nitriding the samples were ground, polished (last step: 1µm diamond paste) and cleaned in an ultrasonic bath filled with ethanol.

3.3.2 Nitriding

For nitriding a sample was suspended at a quartz fibre in a vertical tube furnace. To start the nitriding process the sample was placed in the middle of the nitriding furnace. The nitriding experiments were performed in an ammonia/hydrogen gas flux (purity: H_2: 99.999 vol. %,

NH_3: >99.998 vol. %). The fluxes of both gases were adjusted with mass flow controllers and amounted 9 and 91 ml/min for ammonia and hydrogen, respectively, which corresponds with a nitriding potential $r_n \equiv p_{NH_3}/p_{H_2}^{\frac{3}{2}}$ [4] of about r_n=0.1 atm$^{-1/2}$. The nitriding times for this study have been given in Table 2 for the investigated Fe-Cr alloys.

Table 2: Applied nitriding times at a temperature of 580°C

Fe-4Cr	0.25 h	1 h	2 h	5 h	7 h	15 h	
Fe-7Cr	1 h	4 h	5 h	7 h	10 h	15 h	20 h
Fe-13Cr	7 h	10 h	15 h	20 h	24 h	31 h	48 h
Fe-20Cr	7 h	15 h	20 h	24 h	31 h	48 h	

At the end of the nitiriding process the samples were quenched in water.

3.3.3 Specimen characterisation

3.3.3.1 Microscopy

For light microscopical investigation, pieces were cut from the samples and prepared to cross sections, by subsequent embedding (Konduktomet, Buehler GmbH), polishing (last step: 1 µm diamond paste) and etching with 2.5% nital (2.5 vol.% HNO3 in ethanol) for about 5 s. These cross sections were investigated with light optical microscopy applying a Leica DMRM microscope. The light micrographs were recorded with a digital camera (Jenoptik Progres 3008).

For scanning electron microscopy (SEM) the same (etched) cross-sections were used as for light microscopy. The SEM micrographs were taken with a Jeol JSM 6300F operating at 3 or 5 kV.

3.3.3.2 Hardness measurements

Hardness measurements across the cross-sections of the nitrided specimens were performed with a Leitz Durimet hardness tester, applying a load of 50 g. The presented hardness values are average values of 5 measurements.

3.3.3.3 X-ray diffraction (XRD)

To determine which phases are present after nitriding, XRD was applied using a Philips X'Pert diffractometer. Measurements were made using Cu Kα and Co Kα radiations and employing the Bragg-Brentano geometry with a graphite monochromator in the diffracted beam. The diffraction angle (2Q) range scanned was 10 – 130°, with a step size of 0.05°. The

X-ray diffractograms were recorded from specimen surfaces as obtained after nitriding. To identify the phases from the diffraction peaks the data from the JCPDS data base were used [36].

3.3.3.4 Electron probe microanalysis (EPMA)

To determine the composition of the nitrided zones of the samples after nitriding, EPMA was performed employing a Cameca SX100 instrument. Cross-sections of the nitrided alloys, similar to those as described above for light and scanning electron microscopy, were analysed, but in this case no etching after polishing was applied. A focussed electron beam at an accelerating voltage of 15 kV and a current of 100 nA was applied. To obtain the element contents in the specimens, the intensity of the characteristic Fe Kβ, Cr Kβ, N Kα, and O Kα X-ray emission peaks was determined at points along lines across the cross-sections (single measurement points at a distance of 2 μm). The intensities obtained from the nitrided samples were divided by the intensities obtained from standard samples of pure Fe (Fe Kβ), pure Cr (Cr Kβ), andradite/$Ca_3Fe_2(SiO_4)_3$ (O Kα), and γ'-Fe_4N (N Kα). Concentration values were calculated from the intensity ratios applying the $F(rz)$ approach according to Pouchou and Pichoir (PAP) [37].

3.4 Results and evaluation

Upon nitriding all samples show, for all nitriding times and Cr contents applied, distinct nitrogen uptake, with the exception of the Fe-20Cr alloy nitrided shorter than 5h at 580°C. In chapter 2, it was shown, contrary to practical knowledge, that even for high chromium contents (as 20 wt. %) nitriding at relatively low temperatures is possible, provided an oxygen free atmosphere is applied.

3.4.1 Phase analysis; X-ray diffraction

To determine the phases present in the nitrided zone, X-ray diffractograms were recorded from each nitrided sample. The diffractograms of a Fe-7Cr alloy nitrided for 20h at 580°C and of a Fe-20Cr alloy nitrided for 24h at 580°C are shown in Fig. 3.4.
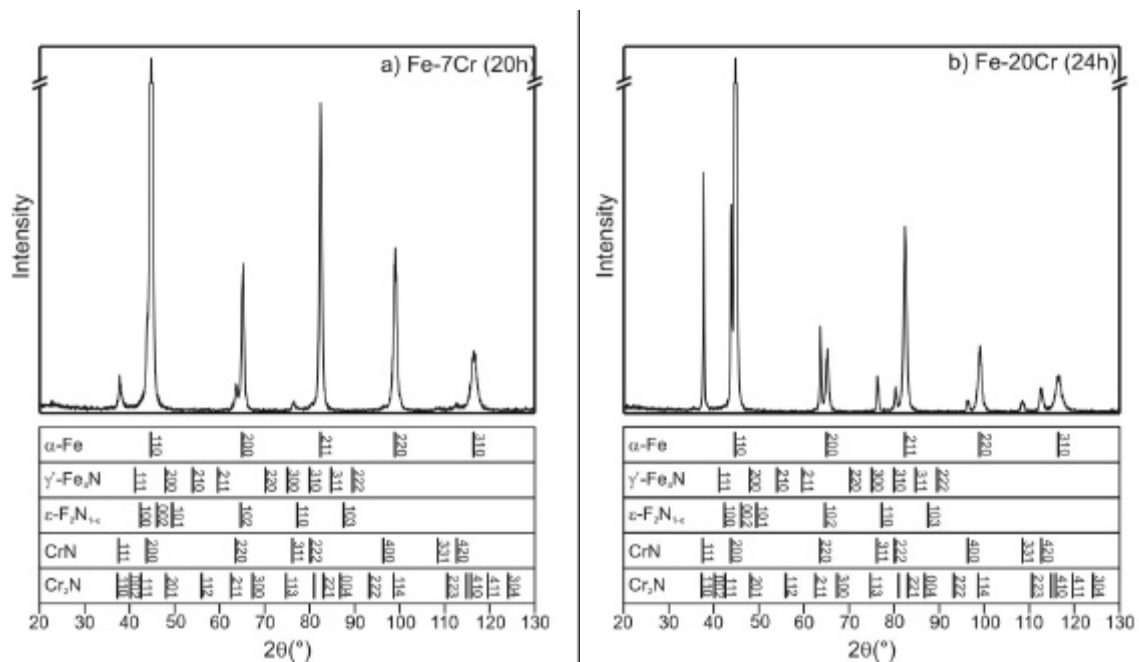
Fig. 3.4: XRD diffractograms of the Fe-7Cr alloy nitrided for 20h at 580°C (a) and the Fe-20Cr alloy nitrided for 24h at 580°C (b).

Clearly, after nitriding only the ferrite (α) and CrN phases are present. As can be expected, the diffractogram of nitrided Fe-7Cr exhibits a lower intensity for the CrN peaks than the diffractogram of the nitrided Fe-20Cr. The occurrence of separate CrN diffraction peaks indicates the presence of relatively coarse CrN particles. This is consistent with the light microscopical results presented below in section 3.4.2 (discontinuous coarsening adjacent to the surface).

3.4.2 Morphologies of the nitrided zone; microscopical investigation

Light micrographs of cross sections of Fe-4Cr, Fe-7Cr, Fe-13Cr and Fe-20Cr specimens nitrided at 580° C for 7h are shown in Fig. 3.5.

In the micrographs of the Fe-4Cr and Fe-7Cr specimen four regions (from the surface to the not nitrided core) can be distinguished:

(i) Mainly near the surface dark grains occur, which show a lamellar morphology in the SEM micrographs (see Fig. 3.5b). In this region the CrN, that has initially been formed as finely dispersed (coherent) precipitates, has (already) been transformed by a

discontinuous coarsening reaction into the lamellar ferrite / CrN morphology (for detailed discussion, see chapter 2 or [21]).

(ii) Below this region bright grains with clearly visible grain boundaries are present. In this region CrN is still present as finely dispersed submicroscopical precipitates within the grains (not visible with SEM), which is consistent with the much higher hardness of these grains as compared to the dark grains. The very pronounced visibility of the grain boundaries is probably caused by preferential formation of CrN precipitates at the grain boundaries and/or the onset of discontinuous transformation at the grain boundaries (see also Ref. 14).

(iii) At larger depths the visibility of the grain boundaries gradually decreases. In this depth range not all Cr has reacted to CrN yet.

(iv) Finally the unnitrided core of the sample follows, where the grain boundaries are not visible anymore. In not nitrided (parts of the) specimens etching does not reveal clearly grain boundaries because the Cr in the specimen causes a protecting Cr_2O_3 layer preventing chemical attack by the etching agent (Figs. 3.5b-d). Obviously this protection is less for the alloy with low Cr content (Fe-4Cr) leading to grain boundary visibility after etching also in the not-nitrided core of this alloy (Fig. 3.5a).

In the micrographs of the Fe-13Cr and Fe-20Cr specimens only two regions can be distinguished, namely the surface adjacent, nitrided region, which has completely been transformed by the discontinuous coarsening reaction, and the unnitrided core. The boundary between the nitrided and unnitrided regions is relatively sharp as compared to the nitrided Fe-4Cr and Fe-7Cr specimens (see also the EPMA results presented in section 3.4.3).

The Fe-20Cr alloys shows a closed nitrided layer only after 5 h of nitriding. This suggests the occurence of an incubation time. Additional nitriding experiments performed on Fe-20Cr alloys for less than 5 hours of nitriding at 580°C showed that the nitriding process starts at isolated locations at the sample surface. At these locations then the discontinuously transformed microstructure, as shown in Fig. 3.5d for a nitriding time of 7h, can already be observed.

The lamellar morphology of the microstructure after discontinuous coarsening is exhibited by Fig. 3.6. The SEM micrograph in Fig. 3.6b shows the occurrence of "subgrains" within a single original grain, characterised by different orientations of lamellae colonies.

Two trends can be indicated for the discontinuous coarsening reaction in dependence on the Cr content:
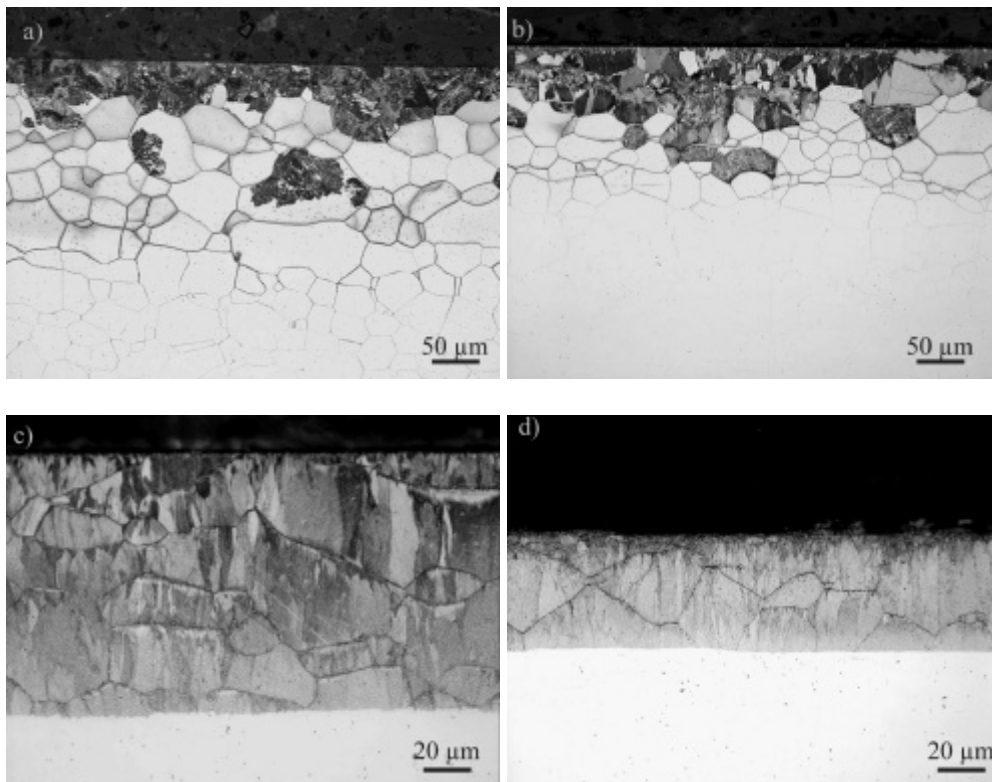

Fig. 3.5: Light micrographs of cross sections of the nitrided Fe-4Cr(a), Fe-7Cr(b), Fe-13Cr (c) and Fe-20Cr (d) specimens. All alloys were nitrded for 7h at 580°C.
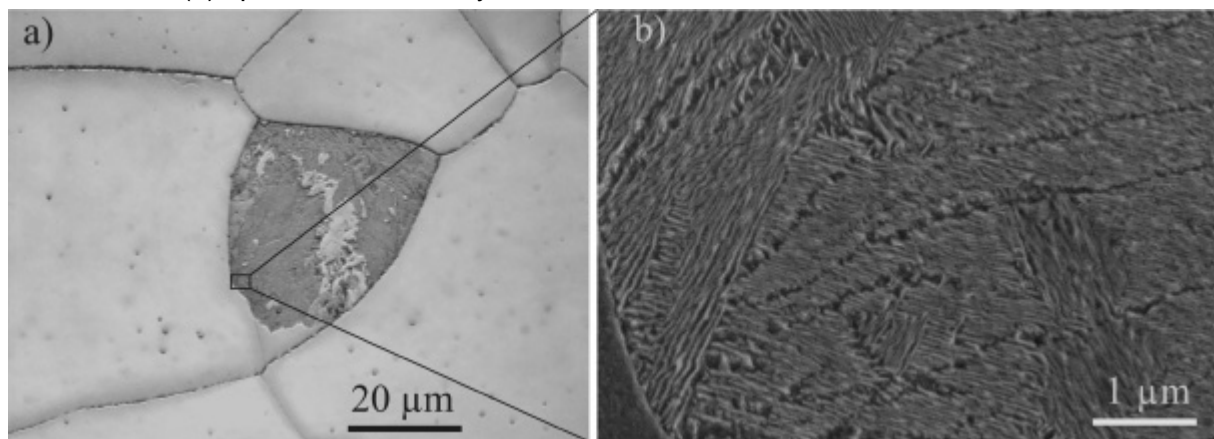

Fig. 3.6: An original grain of the Fe-4Cr alloy after nitriding transformed by the discontinuous coarsening reaction (5h nitriding at 580°C) a) Optical micrograph; b) SEM micrograph of the region indicated in (a). The SEM micrograph reveals the occurrence of many differently oriented colonies of lamellae.

(i)   The amount of discontinously transformed areas increases with the chromium content of the alloy. Whereas the nitrided zones of the Fe-4Cr and Fe-7Cr alloys have only partially transformed discontinously, the nitrided zones of the Fe-13Cr and Fe-20Cr alloys have experienced fully the discontinous coarsening.

(ii)   All discontinuously transformed grains of the nitrided Fe-4Cr alloy show a lot of subgrains (Fig. 3.6b). The discontinuously transformed grains of the nitrided Fe-13Cr and Fe-20Cr alloys show only a few orientations for the lamellae colonies (see Figs. 3.5 c and d and compare with Fig. 3.5 a). In this context, the nitrided Fe-7Cr alloy takes an intermediate position.

Upon performing additional nitriding experiments with Fe-20Cr *single crystals* the same type of discontinuous coarsening morphology occured as observed for the Fe-20Cr polycrystals, except that, obviously, no grain boundaries occurred (see Fig. 3.7).
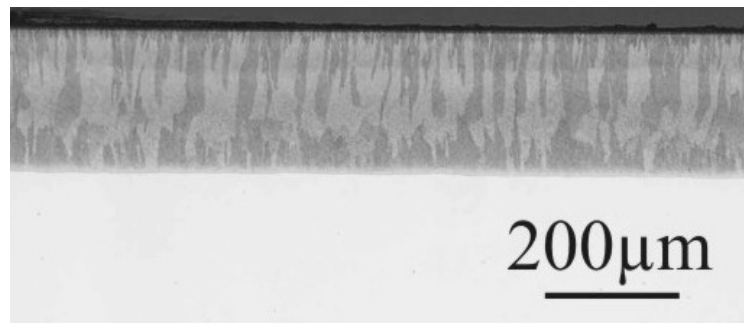

Fig. 3.7: Light micrograph of the cross section of a nitrided Fe-20Cr alloy single crystal nitrided at 580°C with a potential of r_n=0.1 atm$^{-1/2}$ for 48h.

3.4.3 Concentration-depth profiles; EPMA

The nitrogen concentration-depth profiles of the Fe-7Cr alloy nitrided for 7 h at 580°C and of the Fe-20Cr alloy nitrided for 15h at 580°C are presented in Fig. 3.8. The EPMA results obtained for all alloys, reveal an almost constant nitrogen level (plateau) in the nitrided region. Evidently, the higher the chromium contents the larger the nitriding time to reach a similar nitriding depth (cf. Figs. 3.8a and 3.8b). The occurrence of a discontinuously transformed region in the nitrided zone does not influence the nitrogen concentration profile: thus regions (i) and (ii) discussed in Section 3.4.2 cannot be distinguished in the concentration-depth profiles. The region where the nitrogen concentration decreases more or less gradually to zero, corresponds to the transition from nitrided zone to non-nitrided core: region (iii) as indicated in Section 3.4.2, where the visibility of the grain boundaries gradually disappears in the optical micrographs. The width of this region overall decreases with

increasing chromium content (cf. Figs. 3.8a and 3.8b); it does not depend on the nitriding time. The average width of this transition zone (iii) is 31 μm for Fe-4Cr, 24 μm for Fe-7Cr, 8 μm for Fe-13Cr and 13 μm for Fe-20Cr.

It is important to note that the mass ratios of iron and chromium in the nitrided layer and in the not nitrided core, as determined with EPMA, are equal. The change in the (relative) iron and chromium contents across the transition region (iii) is only caused by the decrease of the nitrogen content from nitrided case to non-nitrided core. Hence, (long-range) diffusion of chromium and iron is negligible under the applied nitriding conditions (see further section 4).

The EPMA analysis of all nitrided specimens shows that the nitrogen concentration in the nitrided zone is larger than compatible with (i) the precipitation of all chromium as CrN, and (ii) the equilibrium solubility of nitrogen in the (remaining) ferrite matrix (data in Refs. 4 and 5). The "normal" amount of nitrogen (according to (i) and (ii)), which should be present in the nitrided zone if no excess nitrogen would occur (see sections 3.1 and 3.2), is denoted by the grey lines (see arrow) in Fig. 3.8. Hence, excess nitrogen occurs in the nitrided zone. The "excess nitrogen" is thought to originate partly from the nitrogen attached to (i.e. adsorbed at) the (submicroscopical) nitride platelets in the matrix and partly from dissolved nitrogen in the ferrite matrix strained by the misfit between the (submicroscopical) nitride platelets and the matrix, according to the model described in Ref. 12. The "normal" content of N in the nitrided zone (i.e. the amount of N comparable with precipitation of all Cr as CrN and the equilibrium solubility of nitrogen in the remaining ferrite matrix) has been indicated (arrows in Fig. 3.8).

The influence of the nitriding temperature on the kinetics is shown in Fig. 3.9. The larger penetration depth at higher temperatures is ascribed to two effects (cf. Eqs. (1) and (2)). Firstly, obviously the diffusion coefficient of nitrogen increases with increasing temperature. Secondly, and this is not always recognised, the solubility product K_{MeN_n} normally increases with increasing temperature, which leads to a $c_{N_a}^S$ value increasing with temperature and thus a nitrogen-concentration gradient (in the ferrite matrix) increasing with temperature.
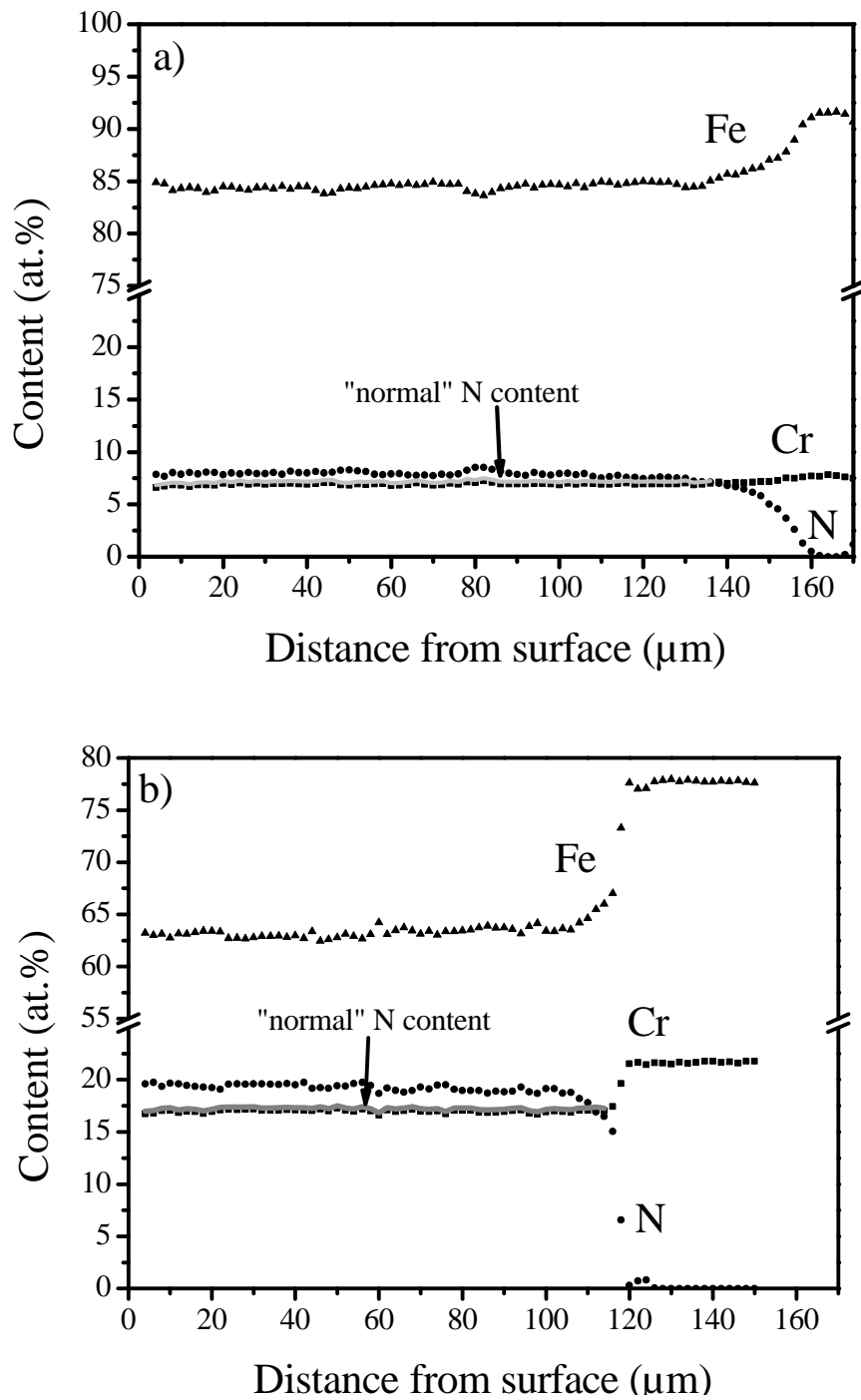
Fig. 3.8: N, Fe and Cr concentration-depth profiles as measured from cross sections by EPMA. a) Fe-7Cr alloy nitrided for 7h at 580°C. b) Fe-20Cr alloy nitrided for 15h at 580°C.
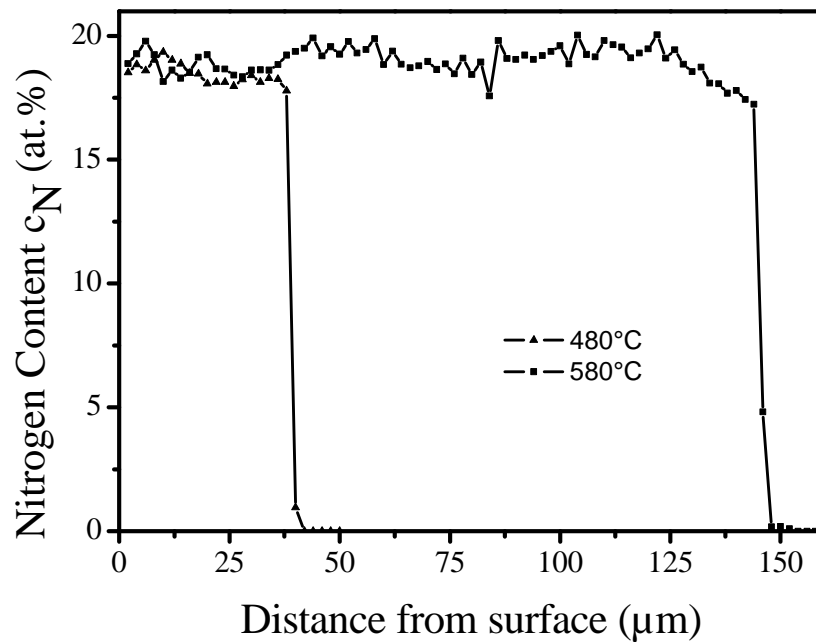
Fig. 3.9: Nitrogen-concentration depth profiles of Fe-20Cr alloys, as measured from cross sections by EPMA, nitrided for 24h at 480°C (grey dots) and for 24h at 580°C (black dots).

The determination of the thickness of the nitrided layers was performed applying light optical micrographs and nitrogen-concentration depth profiles obtained by EPMA analysis of the sample cross sections.

As discussed in section 3.4.2, the nitrdided layers of the Fe-13Cr and Fe-20Cr alloys were completely discontinuously transformed. Therefore the nitrided layer and the not nitrided core can be distinguished very well in optical micrographs (see Figs. 3.5c and d) of the sample. The border between the nitrided layer and the not nitrided core of the Fe-4Cr and Fe-7Cr alloys is not clearly visible in optical micrographs (see Figs. 3.5a and b). Therefore the nitrided layer thicknesses of the Fe-4Cr and Fe-7Cr alloys were determined from the nitrogen-concentration depth profiles. The nitrided layer thickness was taken as the depth where the nitrogen content (in the transition zone) equals half of the Cr content present in the alloy.
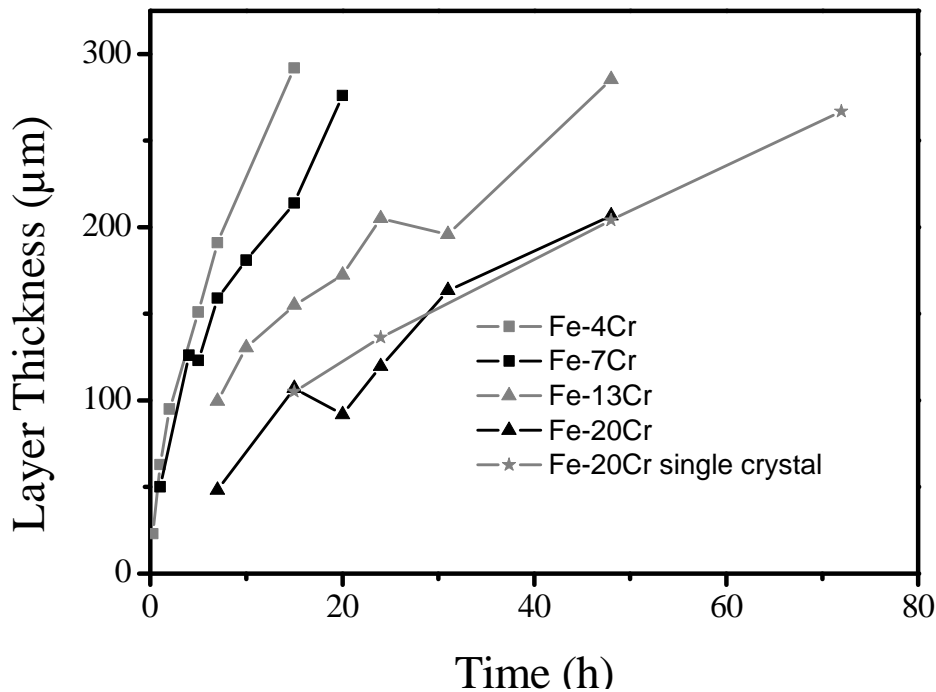
Fig. 3.10: Thickness increase of the nitrided zone in dependence on the nitriding time and the Cr content.

The thickness increase of the nitrided zone in dependence on the nitriding time and the Cr content at 580°C is shown in Fig. 3.10. The Cr content in the sample has a pronounced influence on the growth kinetics of the nitrided zone: the higher the Cr content the smaller the layer thickness. Additionally, the thickness increase as a function of time is shown for nitrided Fe-20Cr single crystals (The stars in Fig. 3.10). The results for the Fe-20Cr single crystal are practically identical to those of the polycrystalline Fe-20Cr material, indicating that the presence of grain boundaries does not have a decisive influence on the growth kinetics of the nitrided zone. The contribution of nitrogen diffusion along grain boundaries can therefore be neglected for the growth of the nitrided zone.

3.5 Analysis of nitriding kinetics

3.5.1 Application of the analytical, approximate model (Eq.(1))

According to Eq. (1), plotting the squared layer thickness vs. nitriding time should yield a straight line. Indeed the present experimental data show this behaviour (Fig. 3.11). The slope of the straight lines is given by $\dfrac{2 \cdot c_N^S \cdot D_N}{c_{Cr}}$ (cf. Eq.(1)).
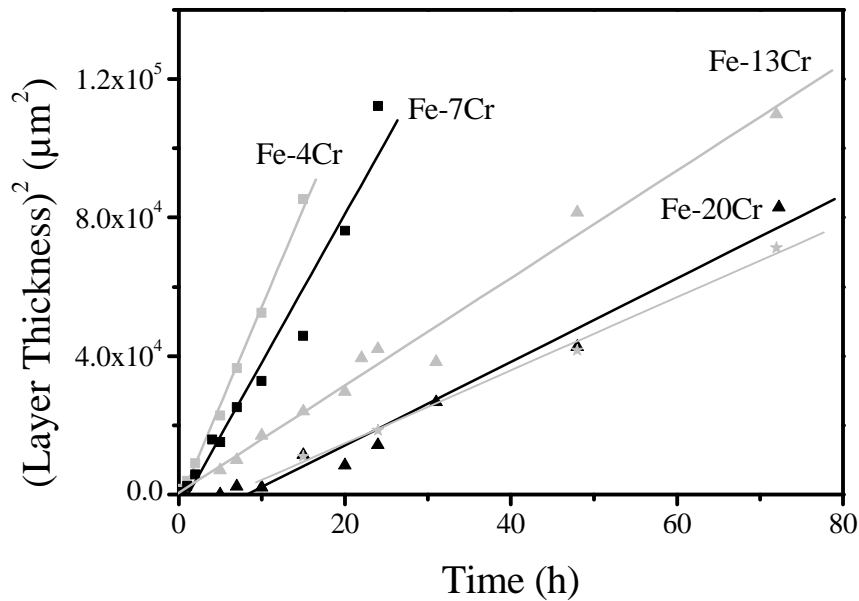
Fig. 3.11: The squared nitrided layer thickness as function of the nitriding time. The straight lines shown are least squares fits to the data of the alloy concerned.

Using literature data for D_N and the known chromium content of the alloy considered, values for $c_{N_a}^S$ can be derived from the slopes. The diffusion coefficient of N in α-Fe at 580°C is 1.14×10^{-7} cm^2/s [38]; the data for c_{Cr} have been given in section 3.3.1. The thus obtained values for $c_{N_a}^S$ are shown in Table 3. They can be compared with the $c_{N_a}^S$ values as obtained experimentally by EPMA (obtained, as average values from the (first) three data points closest to the surface, after subtracting the amount of nitrogen contained in CrN from the total measured N concentration). Furthermore, Table 3 shows the incubation time obtained from the intercept of the fitted straight line with the time axis.

Table 3: Nitrogen solubility in the iron matrix at the surface, $c_{N_a}^S$ as obtained by fitting Eq. (1) to the experimental data and as obtained by EPMA from the time dependent experiments at 580°C.

Alloy:	Fe-4Cr	Fe-7Cr	Fe-13Cr	Fe-20Cr
$c_{N_a}^S$ from straight line fit (at. %):	0.30	0.39	0.26	0.31
$c_{N_a}^S$ from EPMA measurements (at.%):	0.6	1.8	3.8	3.3
incubation time (h):	0.5	0.4	1	7.12

The equilibrium solubility of nitrogen in stress-free ferrite at 580°C and r_n=0.1 (atm$^{-1/2}$), $c_{N_a}^{S,0}$, equals 0.24 at.%, which is lower than the $c_{N_a}^S$ values for dissolved nitrogen at the surface as determined from the straight line fits in Fig. 3.11. This suggests the presence of mobile excess N which contributes to the growth of the nitrided layer (cf. section 3.2). Further, the values of the surface nitrogen content measured by EPMA are much higher than the values for *dissolved* nitrogen at the surface, determined by the straight line fits in Fig. 3.11 according to the analytical model. This (already) suggests the presence of immobile excess nitrogen (nitrogen which is trapped and therefore cannot contribute to the growth of the nitrided layer cf. section 3.2).

3.5.2 Application of the numerical, rigorous model (Eqs. (2)-(5))

Numerically calculated nitrogen depth-profiles, according to Eqs.(2-6) and see Fig. 3.1, were fitted to experimentally determined nitrogen-depth profiles. The fitting parameters are K_{CrN}, b=n+x (with n=1) and $c_{N_a}^S$ (cf. section 3.2). A two step fitting procedure has been applied for the nitrogen-depth profiles measured at 580°C.

The nitrogen-depth profiles have been first fitted individually. The solubility product K_{CrN} (nm^{-6}) should not depend on nitriding time and Cr content at constant temperature. Accordingly, the average value of K_{CrN} (K_{CrN}=0.02 (nm^{-6})) has then been used as a constant in the second, definitive fitting, where only $c_{N_a}^S$ and b were fit parameters. Examples of thus fitted nitrogen-concentration profiles are shown in Fig. 3.12. The results obtained for the surface nitrogen content $c_{N_a}^S$ and the nitride-particle composition parameter b have been gathered in Fig. 3.13 and Table 4.
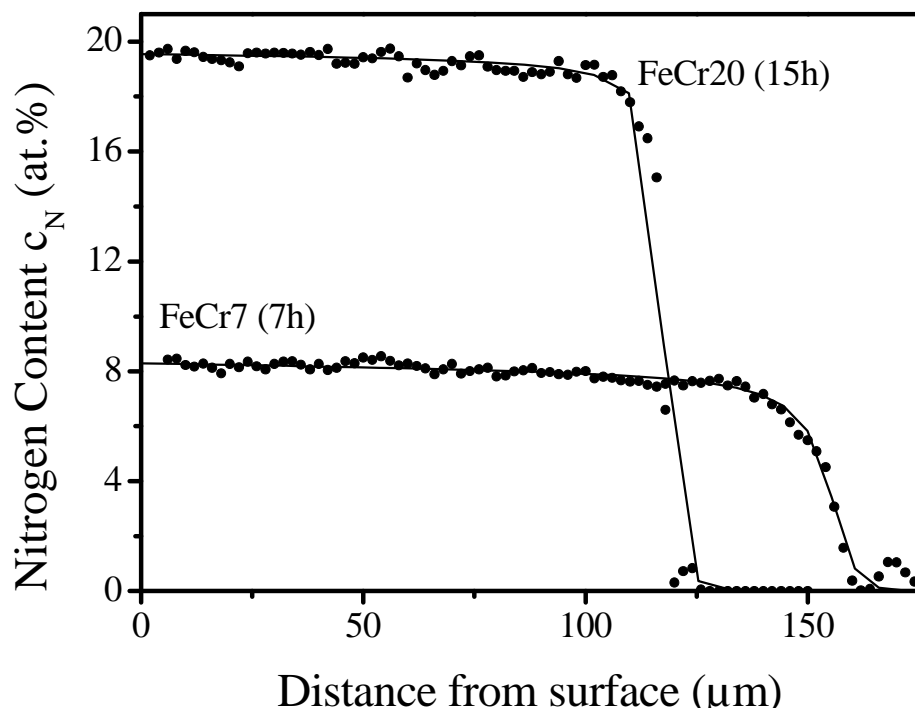
Fig. 3.12: Nitrogen-concentration profiles of nitrided Fe-7Cr and Fe-20Cr alloys, as measured with EPMA (black dots) and as calculated profiles (full lines) by the numerical model applying the parameters: $c_{N_a}^S$ =0.35; b=1.18; K_{CrN}=0.02 (nm^{-6}) for Fe-7Cr and $c_{N_a}^S$ =0.26; b=1.176; K=0.02 (nm^{-6}) for Fe-20Cr.

It follows from Fig. 3.13, that in the case of the Fe-4Cr and Fe-7Cr alloys the surface nitrogen content increases with nitriding time until a saturation level has been reached, whereas the surface nitrogen content of the Fe-13Cr and Fe-20Cr alloys appears to be independent of the nitriding time. Note that to achieve the same nitriding depth, much larger nitriding times are necessary for the Fe-13Cr and Fe-20Cr alloys than for the Fe-4Cr and Fe-7Cr alloys (see Fig. 3.13). The initial increase of $c_{N_a}^S$ (as observed in Fig. 3.13a for the Fe-7Cr and Fe-4Cr alloys) may be due to the finite period of time necessary to establish local equilibrium, at the surface of the substrate, of the gas atmosphere with the solid substrate. This effect has been observed for the nitriding of pure iron and is due to the finite rate of dissociation of NH$_3$ [39]. The effect can be stronger for Fe-Cr, because in the presence of Cr much more N has to be taken up before saturation at the surface has been attained. The solid horizontal lines in Fig. 3.13 represent the average values of the surface nitrogen content as determined from all nitriding times; for the Fe-4Cr and Fe-7Cr alloys only values of samples

which were nitrided longer than 4h were considered to calculate the average value of $c_{N_a}^S$, as for smaller times no saturation at the surface occurs (cf. discussion above). To determine the $c_{N_a}^S$ values of the Fe-20Cr alloys an incubation time of 5h was accounted for (see also Fig. 3.11). This incubation time was determined by metallographical investigation of the cross sections of the nitrided zones. Fe-20Cr alloys nitrided shorter than 5 h do not show a closed nitrided zone (cf.section 3.4.2). The dashed horizontal lines in Fig. 3.13 denote the solubility of nitrogen in the unstrained α-Fe matrix calculated according to the Ref. 5.

After saturation with dissolved N has been realized upon nitriding at 580°C, the solubility of nitrogen in the pure iron matrix of the nitrided Fe-Cr alloys is higher than as expected for pure iron (0.24 at. % [5]). This indicates the presence of *mobile* excess nitrogen (i.e. dissolved nitrogen) that contributes to the (further) growth of the nitrided zone. The average $c_{N_a}^S$ values are presented in Table 4.

The b values for all alloys show, just as the $c_{N_a}^S$ values for the Fe-13 and Fe-20Cr alloys (see Fig 3.13 and above discussion), no systematic dependence on nitriding time. Therefore the time average values of b are shown in Table 4 as function of Cr content. Clearly, b>1, which indicates the presence of *immobile* excess nitrogen in the nitrided zone.

Two explanations for this immobile excess nitrogen may be given:

(i) It may be suggested that this immobile excess N is due to N (originally) adsorbed at the faces of the submicroscopical, coherent nitride particles. At a later stage of nitriding, where practically the whole, or large parts of, the nitrided zone have experienced the discontinuous coarsening reaction, this N may no longer be accommodated at the interface of the CrN (now lamellae) with the α-Fe (now lamellae) and thus this N could have segregated (e.g. at grain boundaries) leading to porosity (N_2 formation), as has been detected ([21] or see chapter 2). Also then, this N cannot contribute to further nitriding and is accounted for in the kinetic model as immobile nitrogen.

(ii) In earlier work on nitrided Fe-Cr [12, 14, 30] it has been concluded that in case of CrN in α-Fe (and in contrast with, e.g., TiN in α-Fe or VN in α-Fe) no nitrogen adsorbs at the faces of the coherent CrN platelets. Further, as compared with the data for $c_{N_a}^S$ obtained here, a much higher value of dissolved excess N has been deduced for an α-Fe matrix containing only submicroscopical, coherent CrN platelets: $c_{N_a}^S$ values more than three times larger than

the equilibrium solubility for α-Fe occur [12, 14]. The present, much lower values for mobile excess N suggest that the largest part of this originally mobile excess N is no longer dissolved in the α-Fe matrix upon continued nitriding (note the pronounced extent of the discontinuous coarsening; see above) and could have segregated (see further under (i)). Thereby this part of the excess nitrogen is accounted for in the kinetic model as immobile nitrogen.

It is striking to observe that the highest mobile and immobile excess nitrogen concentrations occur for the Fe-7Cr alloy. This observation can be interpreted as follows. The occurrence of excess nitrogen is ascribed primarily to the presence of fine, more or less coherent Cr nitride precipitates: large nitride/matrix interfacial area ("trapped" immobile excess nitrogen) and pronounced nitride/matrix misfit-strain fields (dissolved, mobile excess nitrogen). Increase of Cr content in principle leads to more chromium-nitride precipitate phase, which, if all nitride would precipitate in the finely coherent manner indicated above, would lead to an amount of excess nitrogen that increases with the chromium content of the alloy. However, the amount of grains that exhibit the discontinuous coarsening reaction (thought to be associated with lack of capacity for excess nitrogen uptake), also increases with Cr content (see Fig. 3.5). Thus, some optimum Cr content could be imagined that would give the highest amount of excess nitrogen. Apparently, for the present alloy series and the present nitriding conditions, the Fe-7Cr alloy provides such an optimum (cf. Fig. 3.5b).

One may wonder that, in particular for the Fe-13Cr and Fe-20Cr alloys, where the entire nitrided zone has experienced the discontinuous coarsening reaction, the analysis of the growth kinetics yet suggests the occurrence of a significant amount of mobile excess nitrogen that directly influences the growth kinetics. A possible explanation may be that not all Cr is incorporated in the CrN lamellae of the discontinuous precipitation microstructure: a part of the Cr in the specimen may still be present as submicroscopical coherent CrN particles in the remaining α-Fe matrix (α-Fe lamellae), implying, that the discontinuous coarsening did not occur for all Cr (in CrN), as has been confirmed by recent transmission electron microscopical analysis carried out by our group [42].
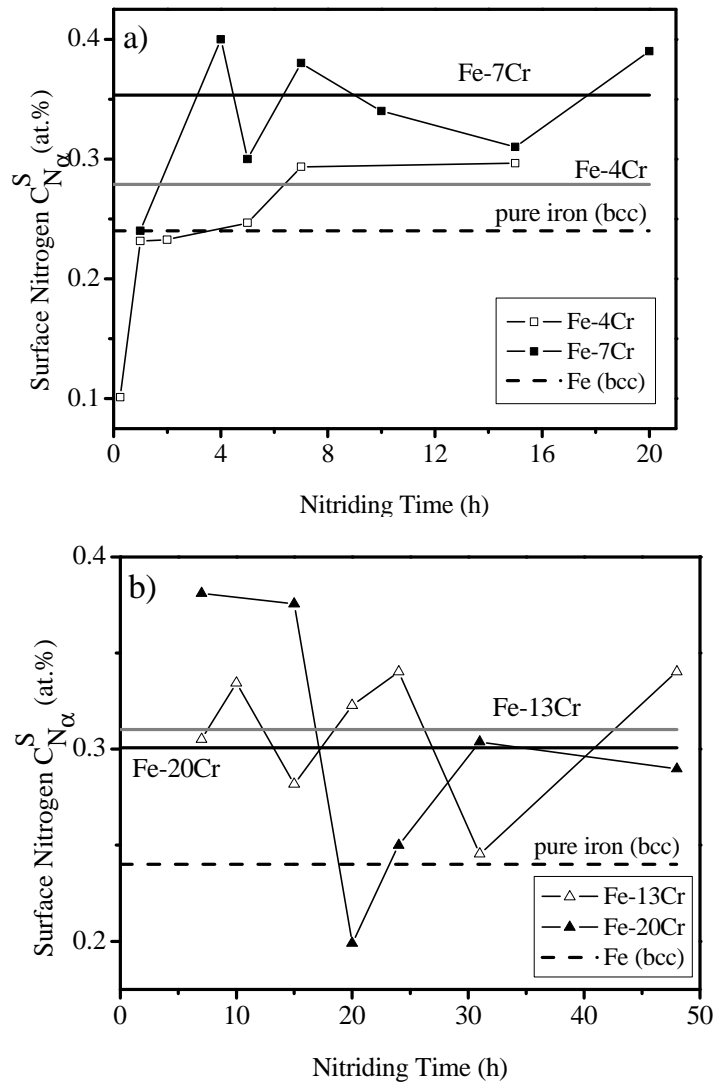
Fig. 3.13: Surface nitrogen concentration, $c_{N_a}^S$, as a function of nitriding time. a) Fe-4Cr and Fe-7Cr alloys. b) Fe-13Cr and Fe-20Cr alloys. The full horizontal lines represent the average c_N values for the alloys indicated (for the Fe-4Cr and Fe-7Cr alloys only values with a nitriding time larger than 4h have been considered). The dashed horizontal lines in both figures indicate the nitrogen solubility of (unstrained) pure iron (bcc) at the applied nitriding conditions.

Table 4: Average values for b=n+x=1+x and $c_{N_a}^S$ in dependence on the Cr content for nitriding at 580°C. In the case of the alloys with 4 and 7 wt. % Cr only the values that were obtained from nitriding times larger than 4h were considered.

Alloy:	Fe-4Cr	Fe-7Cr	Fe-13Cr	Fe-20Cr
$c_{N_a}^S$ (at.%):	0.27	0.35	0.31	0.32
b:	1.06	1.18	1.15	1.11

3.6 Conclusions

(i)   Upon nitriding ferritic Fe-Cr alloys various precipitation morphologies can be observed:

   - initial precipitation of submicroscopical, coherent CrN precipitates in a ferrite matrix;

   - followed by a discontinuous coarsening reaction, involving the development of a (coarse) CrN/α-Fe lamellae structure.

(ii)   The morphology of the nitrided zone depends on the Cr content. The nitrided Fe-4Cr and Fe-7Cr alloys exhibit grains of high hardness containing the fine, dispersed CrN precipitates and, in particular near the surface, grain of low hardness having experienced the discontinuous transformation. The nitrided zones of the Fe-13 and Fe-20Cr alloys are completely discontinuously transformed.

(iii)   In the nitrided zone "excess nitrogen" occurs, i.e. more nitrogen has been taken up than necessary for all Cr to precipitate as CrN and necessary to establish the equilibrium solubility of nitrogen in the ferrite matrix.

(iv)   The development of the nitrogen-concentration depth profile can be described well by a numerical diffusion model that recognizes the presence of

   - immobile excess nitrogen (trapped nitrogen), and

   - mobile excess nitrogen (dissolved in the ferrite matrix).

(v)   The mobile excess nitrogen has a pronounced influence on the nitriding depth (and has a marginal effect on the nitrogen content of the nitrided zone); the immobile excess nitrogen expresses itself primarily through the (higher) nitrogen content of the nitrided zone.

(vi)   An optimum Cr content corresponding to the highest amount of excess nitrogen taken up can occur as the net outcome of two trends:

   - increase of amount of nitride precipitate with increase of Cr content;

   -increase of the extent of the discontinuous coarsening reaction with increase of Cr content.

References

[1]   Mittemeijer, E.J. (ed.): Mat. Sci, Forum 102-104 (1992) 223.

[2]   Wriedt, N.A.; Gocken, R.H.; Nafziger, R.H.: Bulletin of Alloy Phase Diagrams 8 (1987) 355.

[3]   Lehrer, E.: Z. Lektrochem. 36 (1930) 383.

[4]   Mittemeijer, E.J.; Slycke, J.T.: Surface Eng. 12 (1996) 152.

[5]   Mittemeijer, E.J.; Somers, M.A.J.: Surface Eng. 13 (1997) 483.

[6]   Somers, M.A.J.; Mittemeijer E.J.: Metall. Mater. Trans. A26 (1995) 57.

[7]   Du, H. ; Ågren, J.: Z. Metallkd. 8 (1995) 522.

[8]   Du, H. ; Ågren, J.: Du, H; Ågren, J.: Metall. Mater. Trans. A 27 (1996) 1073.

[9]   Torchane, L.; Bilger, P.; Dulcy, J.; Gantois, M.: Metall. Mater. Trans. A 27 (1996) 1823.

[10]   Jack, K.H. in Proc. Conf. on Heat Treatment, The Metals Society, London (1975) 39.

[11]   Mortimer, B.; Grieveson, P.; Jack, K.H.: Scand. J. Metall. 1 (1972) 203.

[12]   Somers, M.A.J.; Lankreijer, R.M.; Mittemeijer, E.J.: Phil. Mag. 59A (1989) 353.

[13]   Imai, Y.; Tsuyoshi, M.; Keikichi, M. : Sci. Rep. Res. Tohoku A19 (1967) 35.

[14]   Hekker, P.M.; Rozendaal, H.C.F.; Mittemeijer, E.J.: J. Mater. Sci. 20 (1985) 718.

[15]   Williams, D.B.; Butler, E.P.: Int. Met. Rev. 26 (1981) 153.

[16]   Permyakov, V.G.; Belotskii, A.V.; Barabash, R.I.: Metallofizika 42 (1972) 102.

[17]   Lightfoot, B.J.; Jack, D.H.: Proceedings on the conference on heat treatment 1973, (The metals society, London 1975), 59-65.

[18]   Mittemeijer, E.J. ; Vogels, A.B.P.; van der Schaaf, P.J.: J. Mater. Sci. 15 (1980) 3129.

[19]   van Wiggen, P.C.; Rozendaal, H.C.F.; Mittemeijer, E.J.: J. Mater. Sci. 20 (1985) 4561.

[20]   Granito, N.; Kuwahara, H; Aizawa T.: J. Mater. Sci. 37 (2002) 835.

[21]   Schacherl, R.E.; Graat, P.C.J.; Mittemeijer, E.J.: Z. Metallkd. 93 (2002) 5.

[22]   Meijering, J.L.: Advances in Material Research 5 (Wiley Interscience, New York, (1971) 1.

[23]   Alves, C; de Anchieta Rodrigues, J.; Eduardo Martinelli, A: Mater. Sci. Eng. 279 (2000) 10.

[24]   Bigliari, M.H.; Brakman, C.M.; Mittemeijer, E.J.; van der Zwaag, S.: Phil. Mag. 72A (1995) 931.

[25]   Jack, D.H.: Acta Metall. 24 (1976) 137.

[26] Podgurski, H.H., Davis, F.N.: Acta Metall. 29 (1981) 1.

[27] Rickerby, D.S.; Henderson, S.; Hendry, A.; Jack, K.H.: Acta Metall. 34 (1986) 1687.

[28] Yang, M.M.; Krawitz, A.D.: Metall. Trans. 15A (1984) 1545.

[29] Podgurski, H.H.; Oriani, R.A., Davis, N.A., with Appendix by Li, J.C.M. and Chou, Y.T.: Trans. Metall. Soc. AIME 245 (1969) 1603.

[30] Mittemeijer, E.J.; Rozendaal, H.C.F.; Colijn, P.F.; van der Schaaf, P.J.; Furnée, R.Th.: Proceedings of the conference on heat treatment 1981, Birmingham, UK, 1981 (The Metals Society London, 1983) 107.

[31] Crank, J.: Mathematics of Diffusion, Clarendon Press, Oxford (1975) 137.

[32] Bongartz, K.; Lupton, D.F.; Schuster, H.: Metall. Trans. 11A (1980) 1983.

[33] Bongartz, K.; Quadakkers, W.J.; Schulten, R.; Nickel, H.: Metall. Trans. 20A (1989) 1021.

[34] Sun, Y.; Bell, T.: Material Science and Engineering 224A (1997) 36.

[35] Gouné, M.; Belmonte, T.; Fiorani, J.M. ; Chomer, S. ; Michele, H.: Thin Solid Films 377-378 (2000) 543.

[36] JCPDS-International Centre for Diffraction Data (1999), PCPDFWIN, Version 202.

[37] Pouchou, J.L.; Pichoir, F.: La Recherche Aérospatiale no. 1984-3 13.

[38] Fast, J.D.; Verrijp, M.B.: Journal of The Iron and Steel Institute 176 (1954) 24.

[39] Rozendaal, H.C.F.; Mittemeijer, E.J.; Colijn, P.F.; Van Der Schaaf, P.J.: Metall. Trans. 14A (1983) 395.

[40] Imai, Y; Masumoto, T.; Maedia, K.: The 1299th report of the Research Institute for Iron, Steel and other Metals. (1967) 35.

[41] Philiips, V.A.; Seybolt, A.U.: Tranas. Metall. Soc. AIME 242 (1968) 2415.

[42] Zieba, P.; Schacherl, R.E.; Mittemeijer, E.J.: to be puplished

4. Zusammenfassung der Arbeit

4.1 Einleitung

Nitrieren ist ein technologisch weit verbreitetes Verfahren zur Verbesserung des Ermüdungsverhaltens, Erhöhung der Verschleißfestigkeit und Verbesserung der Korrosionsbeständigkeit von Bauteilen. Während des Nitriervorganges wird Stickstoff in die Randschicht des zu nitrierenden Werkstoffes gelöst. Von besonderem Interesse ist dabei der Einfluss der Legierungszusammensetzung sowie der angewendeten Nitrierparameter auf die Eigenschaften der Nitrierschicht und der Wachstumskinetik. Damit der Nitrierprozess hinsichtlich der Eigenschaften nitrierter Schichten sowie der Wachstumskinetik optimiert werden kann, ist ein grundsätzliches Verständnis der Vorgänge beim Nitrieren erforderlich. In besonderem Maße wird der Nitriervorgang von den in der Legierung gelösten Elementen und der entstehenden Mikrostruktur beeinflusst.

In der vorliegenden Arbeit soll das Nitrierverhalten von Fe-Cr Legierungen untersucht werden, da Cr in typischen Nitrierstählen enthalten ist. Durch die relativ starke Affinität von Cr zu Stickstoff werden während des Nitriervorganges Chromnitride in der mit Stickstoff angereicherten Nitrierschicht gebildet. Dieser Vorgang ist verknüpft mit der Ausscheidung von fein verteilten Chromnitrid-Plättchen, welche im Anfangsstadium kohärente Grenzflächen zur Eisen-Matrix aufweisen. Bedingt durch die Kohärenz werden Spannungsfelder in die Eisen-Matrix eingebracht, welche wiederum relativ hohe Härten und eine erhöhte Löslichkeit für Stickstoff in der Eisen-Matrix bewirken. Auf Grund der Spannungsfelder und des relativ hohen Grenzflächenanteils Ausscheidung/Matrix findet bei Weiterführung des Nitriervorganges eine Vergröberung der ausgeschiedenen Chromnitride statt. Diese Vergröberung ist verbunden mit dem Abbau der Kohärenz, erkennbar an einem deutlichen Härteabfall. Im System Fe-Cr-N werden zwei Ausscheidungsarten von Chromnitriden beobachtet (i) einzeln ausgeschiedene Chromnitrid Partikel (ii) diskontinuierlich ausgeschiedene lamellenförmig angeordnete Chromnitride. Es wird davon ausgegangen, dass es sich bei der diskontinuierlichen Ausscheidungsstruktur um einen Vergröberungsmechanismus handelt. Es sind daher prinzipiell zwei Vergröberungsmechanismen vorstellbar (i) Vergröberung einzelner Chromnitrid Partikel (ii) Vergröberung durch Ausbildung einer lamellaren Struktur (diskontinuierliche Vergröberung). Das Auftreten beider Varianten wird in der Literatur ausführlich behandelt, allerdings sind

keine Untersuchungen bekannt in denen der systematische Einfluss der Temperatur und des Chromgehaltes auf die Ausscheidungs- bzw. Vergröberungsmorphologie behandelt wird.

Das Auftreten von Ausscheidungen in der Nitrierschicht beeinflusst neben den Eigenschaften auch die Wachstumskinetik der Nitrierschichten. Wie schon zuvor erwähnt erhöht sich bei Chromnitrid-Partikeln mit vollständiger oder teilweiser Kohärenz die Löslichkeit für Stickstoff auf den Oktaederlücken. Darüber hinaus kann zusätzlicher Stickstoff an den Grenzflächen zwischen Ausscheidung und Matrix gelöst werden. Dieser wird in der Literatur als Überschussstickstoff (Englisch: Excess Nitrogen) bezeichnet. Der auf den Oktaederlücken zusätzlich gelöste mobile Stickstoff trägt zum Wachstum der Nitrierschicht bei. Dagegen verringert der an den Grenzflächen adsorbierte (immobile) Überschussstickstoffanteil die Wachstumsgeschwindigkeit der Nitrierschicht, da diese Grenzflächen neben den inneren Nitriden als Stickstoffsenken aufgefasst werden können.

In der Literatur sind bislang Modelle zur Beschreibung der Wachstumskinetik verfügbar, welche die Bildung von inneren Nitriden berücksichtigen. Allerdings wird dabei die Rolle des auftretenden mobilen und immobilen Überschussstickstoffes nicht berücksichtigt.

Zielsetzung dieser Arbeit ist es, einen Beitrag zum grundlegenden Verständnis der Vorgänge beim Nitrieren von Fe-Cr Legierungen zu leisten. Dabei sind zwei Aspekte von Bedeutung, zum einen die Prozess-Optimierung durch Anwendung geeigneter Nitrierparameter und Probenzusammensetzungen, zum anderen die Herstellung von Nitrierschichten mit den gewünschten Eigenschaften. Dazu ist einerseits das Charakterisieren der Mikrostruktur nitrierter Schichten in Abhängigkeit der gewählten Nitrierparameter und Probenzusammensetzung nötig, andererseits die Analyse der Stickstoffkonzentration entlang des nitrierten Querschnitts. Im ersten Kapitel dieser Arbeit soll verstärkt die Mikrostruktur in Abhängigkeit der angewendeten Nitrierparametern und des Cr-Gehaltes untersucht werden. Das zweite Kapitel befasst sich mit der Wachstumskinetik und insbesondere mit dem Einfluss von Überschuss-Stickstoff auf die Wachstumskinetik.

4.2 Experimentelles

4.2.1 Probenherstellung

Fe-Cr Legierungen mit 4, 7, 13 und 20 Gew. % wurden aus reinem Fe (99,98 Gew. %) und reinem Cr (99,999 Gew. %) in Lichtbogen- bzw. Induktionsöfen hergestellt. Die Herstellung der Legierungen im Induktionsofen erfolgte in einem Al_2O_3 Tiegel.

Nach dem Abgießen wurden die Legierungen zu Blechen gewalzt. Anschließend wurden die Bleche in rechteckige Probenstücke geschnitten und unter Schutzgas (Argon mit einer Reinheit von 99.999 Vol. %) bei 700°C für eine Stunde rekristallisiert. Nach dem Rekristallisieren konnte eine mittlere Korngröße von 45µm festgestellt werden.

Mit Hilfe der Elektronenstrahlmikroanalyse konnte gezeigt werden, dass eine homogene Elementverteilung der Legierungsbestandteile in den Legierungen vorliegt. Vor dem Nitrieren wurden die Proben geschliffen, poliert (letzte Stufe: 1µm) und im Ultraschallbad gereinigt.

Das Nitrieren wurde in einem vertikal angeordneten Mehrzonenofen unter einem Ammoniak/Wasserstoff Gasstrom durchgeführt. Die Regelung der Gasströme erfolgte durch „Mass Flow – Controler". Die Nitrierparameter können aus Tabelle 1 Kapitel 2.2.2 u. Tabelle 1 Kapitel 3.3.1 entnommen werden.

4.2.2 Probencharakterisierung

Zur Durchführung der lichtmikroskopischen Untersuchungen wurden Teile der Proben zu Querschliffen präpariert. Zur Querschliffpräparation wurden die Proben eingebettet geschliffen, poliert (letzte Stufe 1µm) und anschließend für 5 Sekunden geätzt (2.5 Vol. % HNO_3 in Ethanol). Die so erhaltenen Querschliffe wurden lichtmikroskopisch untersucht. Die Untersuchungen wurden mit einem Leica DMRM Mikroskop durchgeführt. Die Querschliffbilder wurden mit einer Digitalkamera (Jenoptik Progres 3008) aufgenommen.

4.2.3 Härtemessungen

Härtetiefeprofile wurden entlang der Querschnitte der nitrierten Schichten entnommen. Die Härtemessungen wurden mit einem Leitz Durimet Mikrohärteprüfgerät durchgeführt. Die angewendete Last betrug 50 g.

4.3 Ergebnisse und Diskussion

Im Gegensatz zur allgemeinen Erfahrung war es in dieser Arbeit möglich, Fe-Cr Legierungen mit relativ hohen Cr Konzentrationen bis zu 20 Gew. %, selbst bei relativ niedrigen Temperaturen durch Gasnitrieren aufzusticken. Bei hoch Cr-haltigen Fe-Cr-Legierungen (Cr Konzentrationen > 13 Gew. %) bildet sich an der Oberfläche eine schützende und geschlossene Cr_2O_3-Schicht, welche die Stickstoffaufnahme aus der Ofenatmosphäre behindert bzw. verhindert. Bei hoch Cr-haltigen Stählen ist das Nitrieren daher nur durch physikalische Methoden wie z.B. dem Plasmanitrieren möglich, bei dem Stickstoffatome durch kinetische Energie in die Legierung implantiert werden. Die Nitrierexperimente zu dieser Arbeit wurden unter hochreinen Bedingungen durchgeführt. Es kann daher davon ausgegangen werden, dass sich in der Nitrieratmosphäre (NH_3 / H_2) nahezu kein Sauerstoff befunden hat. Dieser hätte während des Nitriervorganges eine Oxidation an der Oberfläche der zu nitrierenden Probe bewirken können. Da die zu nitrierenden Proben in der Nitrieratmosphäre von Raumtemperatur bis zur gewünschten Nitriertemperatur aufgeheizt worden sind, muss davon ausgegangen werden, dass sich auf Grund der unterschiedlichen Ausdehnungskoeffizienten der Cr_2O_3 Schicht und der Legierung Risse in der schützenden Oxidschicht bilden. An den Rissstellen ist die Aufnahme von Stickstoff in das Substrat (Fe-Cr Legierung) möglich. Die während des Nitrierens entstehenden Spannungen im Substrat ließ die verbleibende Oxidschicht abplatzen. Die Probe konnte somit komplett nitriert werden.

4.3.1 Mikrostruktur des nitrierten Gefüges

Um die Mikrostruktur nitrierter Schichten in Abhängigkeit der Nitrierparameter und der Legierungszusammensetzung zu untersuchen wurden sowohl dünne (100-250 µm) Fe-Cr Folien durchnitriert, als auch nitrierte Schichten in Fe-Cr-Plättchen (1mm dick) hergestellt.

In beiden Fällen konnte die Bildung von Chromnitrid innerhalb des nitrierten Bereiches beobachtet werden (innere Nitrierung). Dabei trat sowohl für alle untersuchten Legierungen (mit 4 – 20 Gew. %), als auch bei allen angewendeten Nitriertemperaturen (450, 580 und 700°C), Chromnitrid mit Steinsalzstruktur (Stöchiometrie 1:1) auf. Das während des Nitriervorganges entstehende Chromnitrid scheidet sich aus der übersättigten Grundmatrix aus, welche aus Ferrit mit gelöstem Cr und N besteht. Dabei können zwei unterschiedliche Ausscheidungsmodifikationen beobachtet werden. Im Anfangsstadium entstehen fein verteilte Chromnitrid-Plättchen, welche mit der Ausgangsmatrix kohärent und/oder teilkohärent sind.

Diese Ausscheidungsform bewirkt auf Grund der Kohärenz und der damit verbundenen Spannungsfelder relative hohe Härtewerte (für nitrierte Fe-Cr-Legierungen typischerweise >1000 HV). Aufgrund der hohen Grenzflächenenergien sowie die durch die Kohärenz bedingten Spannungsfelder stellt dieser Zustand keine Gleichgewichtssituation dar. Eine Vergröberung des ausgeschiedenen Chromnitrids kann dabei entweder durch Wachstum der bestehenden Chromnitrid Partikel oder durch diskontinuierliche Vergröberung erfolgen (siehe Kapitel 4.1). Bei der diskontinuierlichen Vergröberung werden entlang einer Wachstumsfront die ursprünglich feinen (kohärenten od. teilkohärenten) Chromnitrid Teilchen in ein gröberes, lammelares Gefüge überführt, bestehend aus Chromnitrid und Ferrit Lamellen. Diskontinuierlich vergröberte Bereiche können in rasterelektronenmikroskopischen Aufnahmen an der lamellaren Morphologie erkannt werden (siehe Abb. 4.1 b)). Bei mit Nital angeätzten Proben sind in lichtmikroskopischen Aufnahmen diskontinuierlich vergröberte Bereiche an der dunklen Färbung zu erkennen (siehe Abb. 4.1 a) sowie Abb. 4.2).
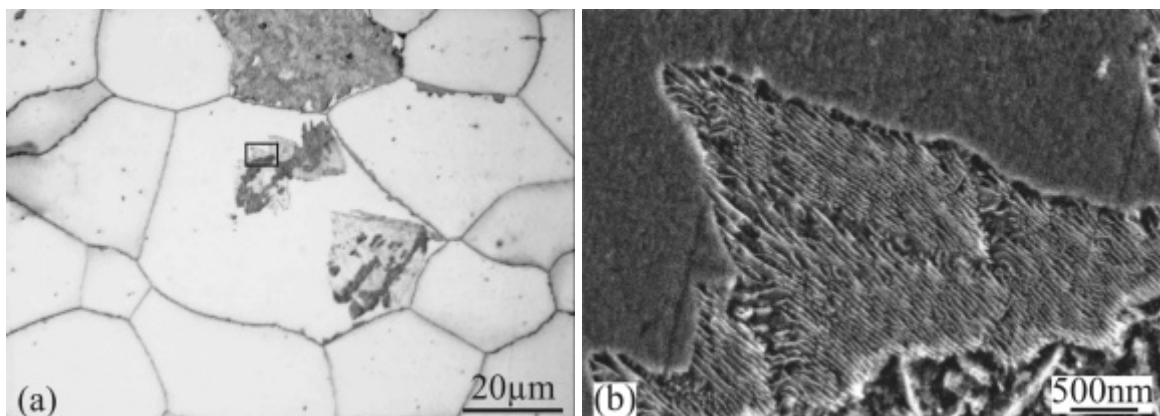
Abb. 4.1: Lichtmikroskopische Aufnahme einer bei 580°C nitrierten Fe-4Cr Legierung (a) sowie eine aus dem in Abb. a) gekennzeichneten Bereich entnommene rastelektronenmikroskopische Aufnahme bei höherer Vergrößerung (b).

4.3.1.1 Mikrostruktur in Abhängigkeit der Nitriertemperatur

Diskontinuierliche Vergröberung tritt vorzugsweise bei relativ niedrigen Nitriertemperaturen auf. Abbildung 4.2 zeigt lichtmikroskopische Aufnahmen von Fe-4Cr bzw. Fe-7Cr Legierungen, welche bei unterschiedlichen Temperaturen nitriert wurden. Deutlich zu erkennen sind diskontinuierlich umgewandelte Bereiche (siehe Abb. 4.2 a)-d)). Erwartungsgemäß sinkt der diskontinuierlich vergröberte Anteil des Gefüges mit steigender Temperatur (vergl. Abb. 4.2 a) u. b) mit c) und d)).
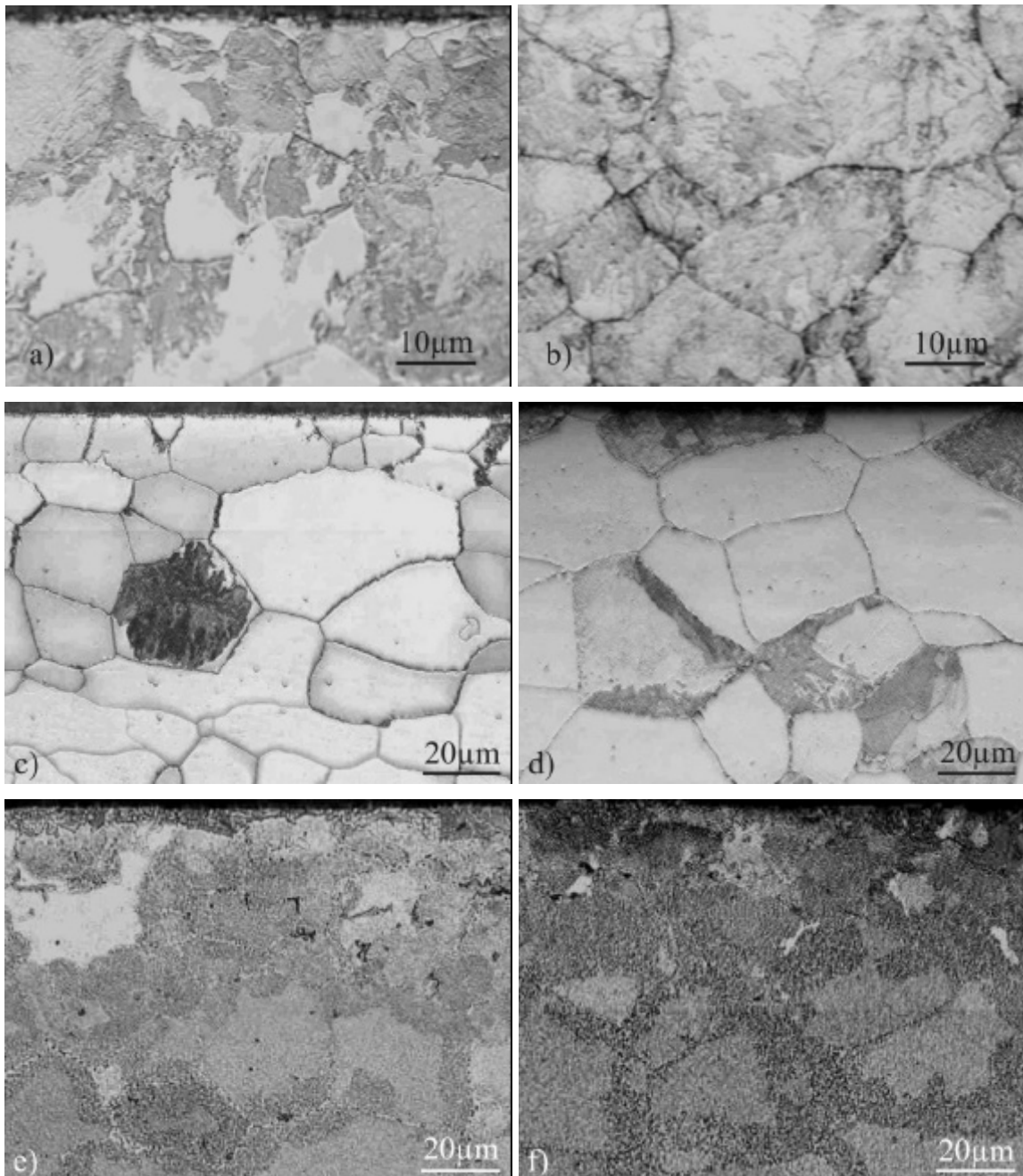
Abb. 4.2: Lichtmikroskopische Aufnahme der bei 450°C für 55h nitrierten Fe-4Cr Legierung (a). Lichtmikroskopische Aufnahme der bei 450°C für 19h nitrierten Fe-7Cr Legierung. c) Fe-4Cr Legierung nitriert bei 580°C für 16h. d) Fe-7Cr Legierung nitriert bei 580°C für 18h. e) Fe-4Cr Legierung nitriert bei 700°C für 18h. f) Fe-7Cr Legierung nitriert bei 700°C für 18h.

Dies ist darauf zurückzuführen, dass bei höheren Nitriertemperaturen (hier T=580°C) eine schnellere Vergröberung der ausgeschiedenen CrN Partikel über Volumendiffusion erfolgt (kontinuierliche Vergröberung). Die Triebkraft zur diskontinuierlichen Vergröberung wird mit steigender Temperatur geringer. Entsprechend weisen die bei 700°C nitrierten Fe-Cr-

Legierungen mit 4, 7, 13 u. 20 Gew. % Cr keine diskontinuierlich vergröberten Bereiche auf. In diesem Temperaturbereich spielt die Volumendiffusion von Cr bereits eine erhebliche Rolle. Die kontinuierliche Vergröberung der ausgeschiedenen CrN Partikel läuft relativ schnell ab, und damit sowohl der Abbau von Grenzfläche zwischen Matrix und Ausscheidung, als auch die durch Kohärenz induzierten Spannungsfelder. Die treibende Kraft zur Vergröberung der Ausscheidungsstruktur wird daher relativ schnell reduziert. Der Mechanismus einer diskontinuierlichen Vergröberung ist auf Grund der beschleunigten Diffusion von Chrom nicht notwendig. Rastelektronenmikroskopische Aufnahmen betätigen die Präsenz von vergröberten CrN Partikeln.

4.3.1.2 Mikrostruktur in Abhängigkeit des Cr Gehaltes

Erheblichen Einfluss auf die Ausscheidungsmorphologie nitrierter Schichten hat der Cr-Gehalt der Ausgangslegierung. Die Untersuchung der Abhängigkeit des Cr-Gehaltes wurde anhand von nitrierten Schichten mit einer Dicke von ca. 20 bis 150 µm durchgeführt. Dabei wurden Bleche mit einer Stärke von 1mm nitriert. Untersucht wurden Fe-Cr Legierungen mit 4, 7, 13 und 20 Gew. %. Abbildung 4.3 zeigt lichtmikroskopische Aufnahmen von Querschliffen nitrierter Schichten (nitriert bei T=580°C, r_n=0.1 atm$^{-1/2}$ und t=7h). Die Nitrierschicht der Fe-4Cr und Fe-7Cr Legierungen können in 4 Zonen unterteilt werden (Abb. 4.3 a) u. b)).

 (i) Direkt unter der Probenoberfläche treten Körner mit dunkler Färbung auf. In diesen Körnern hat eine diskontinuierliche Vergröberung des kohärent oder teilkohärent ausgeschiedenen Chromnitrids stattgefunden.

 (ii) Unterhalb dieser Schicht treten helle Körner mit stark ausgeprägten Korngrenzen auf. Diese Körner zeichnen sich durch eine relativ hohe Härte aus (1200 HV). Verursacht werden diese hohen Härtewerte von fein verteilten Chromnitrid-Ausscheidungen die vollständige Kohärenz oder Teilkohärenz zur umgebenden Matrix besitzen. Bedingt durch die Kohärenz werden Spannungsfelder in der Matrix erzeugt, welche die Versetzungsbewegung behindern, was die relativ hohe Härte erklärt. Die stark ausgeprägten Korngrenzen können durch bevorzugte Chromnitrid Ausscheidungen an den Korngrenzen oder durch das Anfangsstadium der diskontinuierlichen Vergröberungen verursacht werden.

(iii) In der darauf folgenden Zone nimmt der Kontrast der Korngrenzen mit zunehmender Probentiefe ab. In dieser Zone sinkt der Stickstoffanteil auf die ursprüngliche Stickstoff-

Konzentration der zu nitrierenden Probe. Entsprechend sinkt der Anteil an Chrom, welcher sich mit Stickstoff zu Chromnitrid umgesetzt hat.

(iv) Zuletzt folgt der nicht nitrierte Kern der Probe. In diesem Bereich können keine Korngrenzen mehr beobachtet werden. Ausgenommen die nitrierte Fe-4Cr Legierung, in der auf Grund dem fehlenden Schutz einer Cr_2O_3 Schicht das Ätzmittel auch im nicht nitrierten Bereich die Korngrenzen angreift.

In den Abbildungen 4.3c) und d) der Fe-13Cr u. Fe-20Cr-Proben können zwei Regionen unterschieden werden. Eine nitrierte Schicht, die komplett diskontinuierlich umgewandelt ist, und den nicht nitrierten Kern der Probe. Die Grenze zwischen beiden Bereichen weist einen relativ scharfen Übergang auf, im Vergleich zu den Fe-4Cr und Fe-7Cr Proben. Die Dicke der nitrierten Schichten ist innerhalb einer Probe konstant.
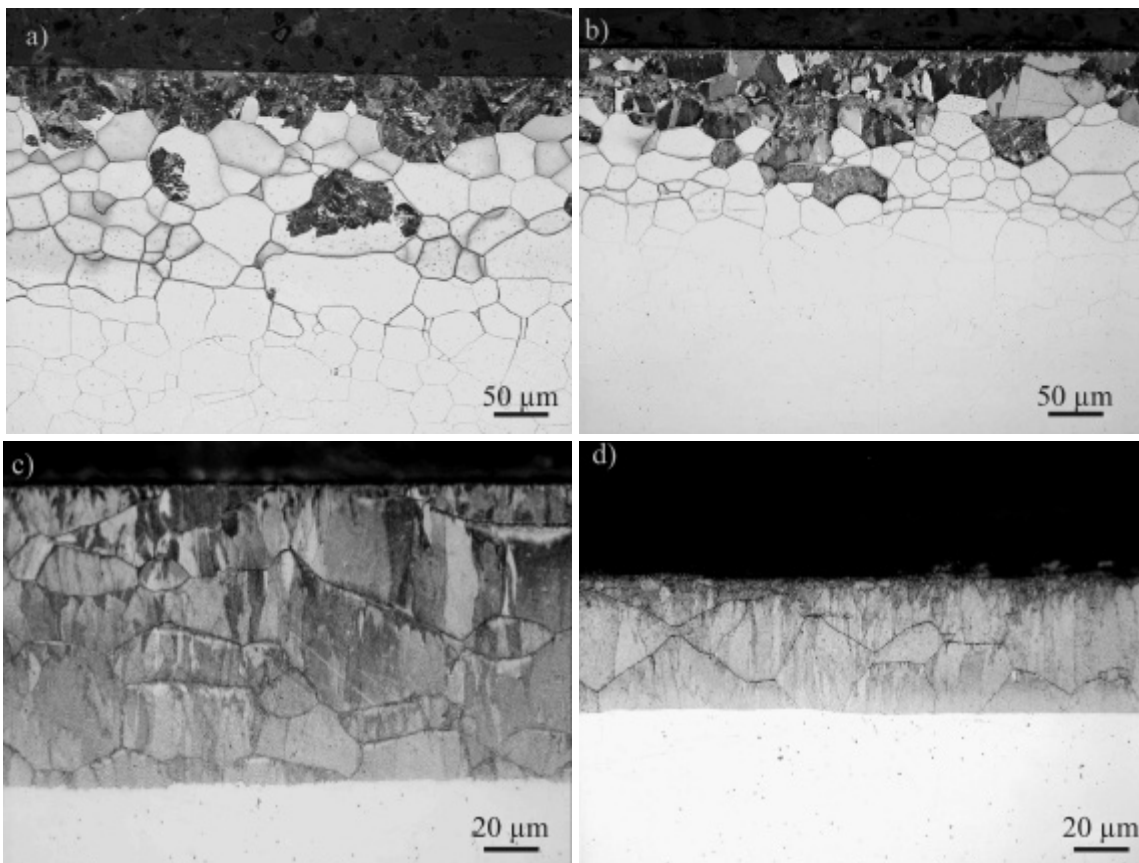
Abb 4.3: Lichtmikroskopische Aufnahmen von Querschliffen nitrierter (t=7h) Legierungen: a)Fe-4Cr; b) Fe-7Cr; c) Fe-13Cr; d) Fe-20Cr.

Es treten neben den relativ groben CrN-Lamellen und CrN-Partikeln (nicht sichtbar im Lichtmikroskop und Rasterelektronenmikroskop), auch Unterschiede der Morphologie innerhalb diskontinuierlich vergröberter Bereiche auf, diese sind vom Cr Gehalt der

Ausgangslegierung abhängig. Nitrierte Schichten in Fe-4Cr Legierungen weisen in diskontinuierlich vergröberten Körner eine Vielzahl von Lamellen-Orientierungen auf. Jeder dieser Orientierungen bildet innerhalb eines diskontinuierlich umgewandelten Kornes ein Subkorn aus (siehe Abb. 4.4 a) u. b)).
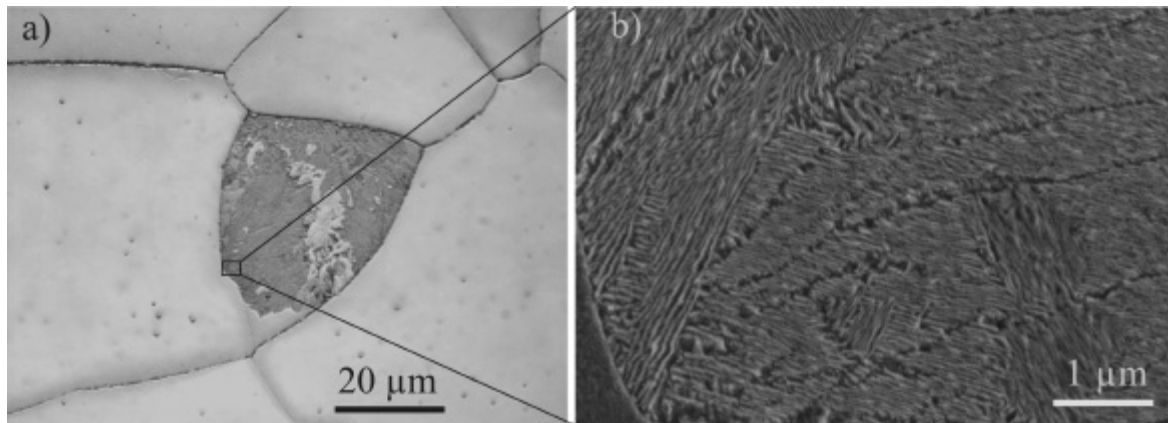

Abb. 4.4: Diskontinuierlich umgewandeltes Korn in einer nitrierten Fe-4Cr Legierung: a) Lichtmikroskopische Aufnahmen; b) Rasterelektronenmikroskopische Aufnahme von dem in Abb. a) gekennzeichneten Bereich.

In den nitrierten Schichten der Fe-7Cr Legierungen treten sowohl diskontinuierlich umgewandelte Körner mit vielen Lamellenorientierungen und Körner mit nur ein oder zwei Orientierungen auf. In den komplett diskontinuierlich umgewandelten nitrierten Schichten der Fe-13Cr und mFe-20Cr Legierungen treten nur Körner mit ein oder zwei Lamellenorientierungen auf. Daraus resultiert eine Systematik zwischen Cr Gehalt in der Ausgangslegierung und der Anzahl der Lamellenorientierung innerhalb eines diskontinuierlich umgewandelten Kornes.

4.3.2 Wachstumskinetik nitrierter Schichten

Die Geschwindigkeit mit der Stickstoff (gelöst auf Oktaederlücken der Ferrite Matrix) in die Probe eindringet hängt ab von (i) äußeren Faktoren wie den Nitrierparametern (Nitrierpotential r_n, Nitriertemperatur und Gaszusammensetzung der Nitrieratmosphäre), sowie (ii) der Zusammensetzung der Probe. Setzt man thermodynamisches Gleichgewicht zwischen Probenoberfläche und der Nitrieratmosphäre voraus, kann die Löslichkeit des Stickstoffes an der Probenoberfläche durch Variation der Nitrierparameter eingestellt werden. Ist Cr in der Ausgangslegierung gelöst, bilden sich während des Nitrierens innere Nitride (siehe Kapitel 4.1). Für die in dieser Arbeit angewendeten Nitrierparameter erhält man eine Nitrierschicht aus Ferrit und CrN (mit NaCl Struktur). Die Formation innerer Nitride bedingt den Verbrauch von gelöstem Stickstoff. Da der zu Nitrid umgesetzte Stickstoff nicht mehr frei beweglich ist, und damit nicht mehr zum Wachstum der Nitrierschicht beitragen kann, muss dieser Sachverhalt in einem die Wachstumskinetik beschreibenden Modell berücksichtigt werden. In einem analytischen Modell, welches ursprünglich zur Beschreibung von innerer Oxidation vorgeschlagen wurde, wird von der stark vereinfachenden Annahme ausgegangen, dass die komplette Umsetzung des in der Grundmatrix gelösten Chroms und Stickstoffes zu Chromnitrid alleine und komplett an der Grenzfläche zwischen nitrierter Schicht und nicht nitriertem Kern der Probe stattfindet. In dieser vereinfachenden Betrachtung wurde weder der Einfluss von Überschussstickstoff, noch die Tatsache, dass in einem Realsystem nicht der gesamte Anteil des gelösten Chroms zu Chromnitrid umgesetzt wird, betrachtet.

Um eine realistischere Beschreibung der Wachstumskinetik nitrierter Schichtung zu erhalten wurde ein numerisches Modell eingeführt. Das Modell basiert auf den folgenden Annahmen:

− Die Eindiffusion von Stickstoff wird durch die 2. Fick'sche Gleichung beschrieben (Lösung durch ein Finite Differenz Ansatz).

− Falls die Konzentrationen von Stickstoff und Chrom lokal ein vorgegebenes Löslichkeitsprodukt K überschreitet wird an der entsprechenden Stelle die Ausscheidung von CrN simuliert, bis die Konzentrationen des gelösten Stickstoffes und Chroms dem Löslichkeitsprodukt K entsprechen. Bei der weiteren Berechnung der Eindiffusion des Stickstoffes wird nur der in Lösung verbleibende Stickstoff berücksichtigt.

Mit diesem Modell ist es daher möglich innere Nitrierung in der Nitrierschicht zu berücksichtigen. Die Berechnung von Stickstofftiefenprofilen ist daher möglich. Dabei müssen zwei Parameter vorgegeben werden: (i) die Oberflächenkonzentration des interstitiell gelösten Stickstoffes c_N^S sowie (ii) das Löslichkeitsprodukt K.

Die nitrierte Schicht vermag zusätzlichen Stickstoff zu lösen (siehe Kapitel 4.1). Dieser zusätzlich gelöste Stickstoff kann sowohl an Spannungsfelder lokalisiert sein (mobiler Überschussstickstoff), sowie an den Grenzflächen zwischen den Chromnitridausscheidungen und der Grundmatrix (immobiler Überschussstickstoff). Das Auftreten von Überschussstickstoff muss bei der Berechnung von Stickstofftiefenprofilen berücksichtigt werden. Dies geschieht indem der Oberflächenstickstoffgehalt c_N^S erhöht wird, wodurch erhöhte Stickstofflöslichkeit in der Grundmatrix simuliert wird, und somit die Präsenz von mobilem Überschussstickstoff. Die Berücksichtigung des immobilen Überschussanteiles erfolgt durch die Einführung eines Parameters b. Dieser Parameter ändert die stöchiometrische Zusammensetzung der inneren Nitride (CrN$_b$) im numerischen Modell, während im Realsystem eine NaCl Struktur vorliegt. Damit kann z.B. für b>1 eine erhöhte Stickstoffaufnahme in der Nitrierschicht simuliert werden. Der dabei zusätzlich gelöste Stickstoff kann nicht mehr zum Wachstum der Nitrierschicht beitragen und ist somit immobil. Der Einfluss des Überschussstickstoffes auf die Wachstumskinetik ist in Abbildung 5 illustriert. In dieser Arbeit konnte durch anpassen gerechneter Stickstofftiefenprofile an gemessene Stickstofftiefenprofile gezeigt werden, dass sowohl mobiler wie auch immobiler Überschussstickstoff in den nitrierten Schichten aller untersuchter Fe-Cr-Legierungen vorhanden ist. Die Anpassung erfolgte, indem zunächst alle Parameter (c_N^S, b und K) variiert wurden. Das Löslichkeitsprodukt K ist unabhängig von Nitrierdauer und Cr-Gehalt der Legierung. Nach der ersten Anpassung wurde der Mittelwerte des Anpassungsparameters K für alle Proben ermittelt. Bei der nächsten und endgültigen Anpassung wurde der zuvor ermittelte Durchschnittswert für K als fester Startparameter bei allen Anpassungen vorgegeben. Anpassungsparameter waren der Oberflächenstickstoffgehalt c_N^S, sowie der stöchiometrische Parameter b, welcher die Anwesenheit von immobilem Stickstoff berücksichtigt. Exemplarisch ist das Resultat der Anpassungen an nitrierten Fe-7Cr und Fe-20Cr Legierungen in Abbildung 4.6 gezeigt.
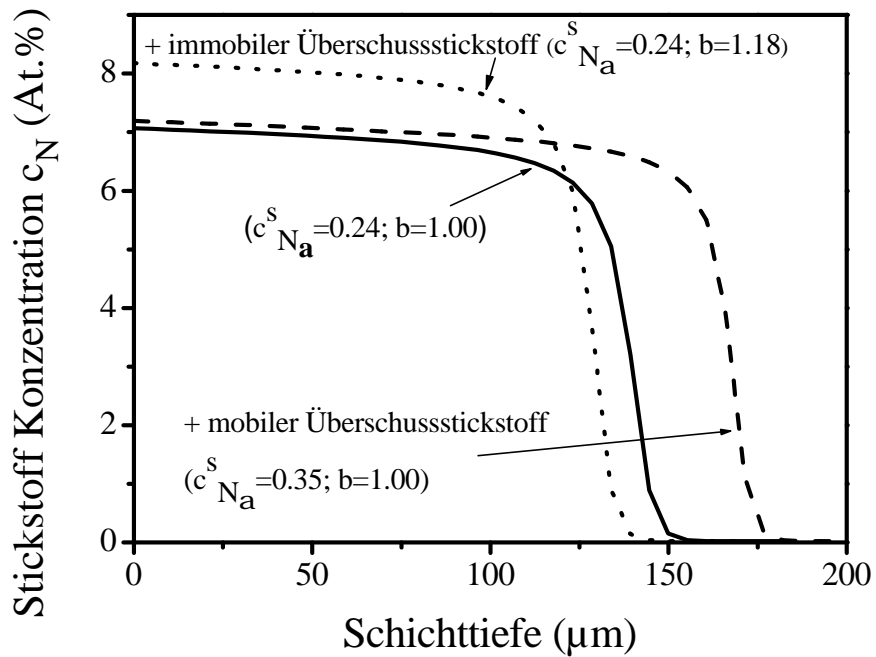
Abb. 4.5: Einfluss des Überschusstickstoffs auf das Stickstofftiefenprofil. Das Profil mit der durchgezogenen Linie entspricht dem Stickstofftiefenprofil ohne Berücksichtigung von Überschussstickstoff.
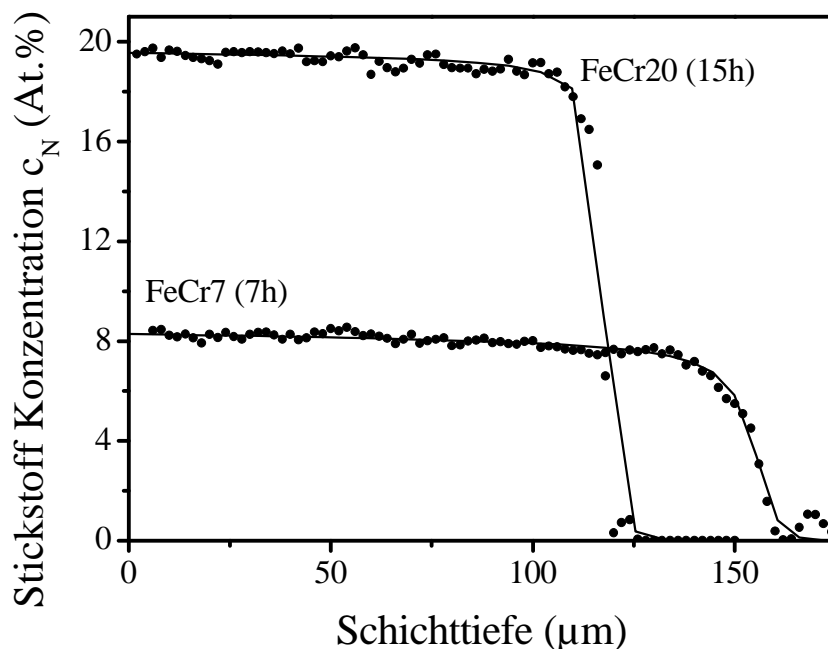

Abb. 4. 6: Anpassung gerechneter Stickstofftiefenprofile an gemessene (Mikrosondenanalyse) Stickstofftiefenprofile einer nitrierten Fe-7Cr und Fe-20 Cr Legierung

Für die Anpassungsparameter ergaben sich die in Tabelle 1 dargestellten Werte.

Tabelle 1: Durchschnittswerte für b=n+x=1+x und $c_{N_a}^S$ in Abhängigkeit des Cr Gehaltes für Proben nitriert bei 580°C.

Cr Konzentration (Gew.%):	4	7	13	20
c_N^S (At.%):	0.27	0.35	0.31	0.32
b	1.06	1.18	1.15	1.11

Bei der Nitrierung von reinem Eisen (Ferrit), unter Verwendung der in Kapitel 3.3.2 angewendeten Nitrierparameter, treten keine Eisennitride auf. Nitrierte Schichten bestehen in diesem Fall lediglich aus einer Ferrit-Matrix, in der Stickstoffatome auf Oktaederlücken gelöst sind. Aufgrund der Abwesenheit von inneren Nitriden (z.B. Chromnitride) tritt kein Überschussstickstoff auf. Die Löslichkeit von Stickstoff in reinem Eisen (Ferrit) beträgt 0.24 At. %. Vergleicht man die für Ferrit zu erwartende Stickstofflöslichkeit mit den aus der Anpassung resultierenden Oberflächenstickstoffkonzentrationen, ergeben sich deutlich höhere Werte für die aus der Anpassung ermittelnden Konzentrationen. Die im Modell als Startparameter vorgegebenen Oberflächenstickstoffkonzentrationen beschreiben den Anteil an Stickstoff, welcher auf den Oktaederlücken gelöst und somit zum Wachstum der Nitrierschicht durch Diffusion beitragen kann. Dieser Stickstoffanteil ist daher als mobil zu betrachten. Bei der Differenz zwischen dem aus der Anpassung ermitteltem Oberflächenstickstoffgehalt und der Löslichkeit von Stickstoff in Ferrit handelt es sich um mobilen Oberflächenstickstoff. Ebenso weisen die aus der Anpassung resultierenden b-Werte (b<1) auf die Präsenz von immobilen Überschussstickstoff hin.

In dieser Arbeit konnte auf Basis kinetischer Modelle gezeigt werden, dass bei dem Wachstum nitrierter Schichten sowohl der Einfluss von mobilem als auch immobilem Überschussstickstoff berücksichtigt werden muss.

Curriculum Vitae

Name	Ralf Erich Schacherl
Date of birth	10.08.1970
Place of birth	Künzelsau

School

1977-1986
Grund und Hauptschule Ingelfingen

1986-1988
Gewerblich-technische Berufsfachschule

1988-1991
Technisches Gymnasium Öhringen

Military Service

1991-1992
- 6. Sanitätsbataillon 310 Marburg
- Heeresfliegerversorgungsstaffel 305

Higher Education

1992-1999
Materials Science at Universität Stuttgart

since 1999
PhD Student at Max-Planck Institut für
Metallforschung and Institut für Metallkunde
of Universität Stuttgart

Danksagung